Spintronic semiconductor devices based on Mn doped GaAs

Natalia Lebedeva

Spintronic semiconductor devices based on Mn doped GaAs

Natalia Lebedeva

Doctoral dissertation for the degree of Doctor of Science in Technology to be presented with due permission of the School of Electrical Engineering for public examination and debate in the Large Seminar Hall of Micronova at the Aalto University School of Electrical Engineering (Espoo, Finland) on the 15th of November 2013 at 12 noon.

Aalto University
School of Electrical Engineering
Department of Micro and Nanosciences
Electron Physics Group

Supervising professor
Professor Pekka Kuivalainen

Thesis advisor
Dr. Sergey Novikov

Preliminary examiners
Professor Magnus Wilander, Linköping University, Sweden
Professor Jouni Ahopelto, VTT Information technology, Finland

Opponent
Professor Ronald Österbacka, Åbo Akademi, Finland

NORDIC ECOLABEL

441   697
Printed matter

Author
Natalia Lebedeva

Name of the doctoral dissertation
Spintronic semiconductor devices based on Mn doped GaAs

Abstract

  The effects of the strong sp-d exchange interaction, ferromagnetic ordering and large spin fluctuations on the electrical transport properties of various spintronic semiconductor devices have been studied both theoretically and experimentally. The studied devices, which either have a ferromagnetic Mn doped GaAs layer or a Mn doped quantum dot as a central part of the device structure, included pn- and Schottky diodes, Esaki-Zener tunnel diodes, resonant tunnelling diodes, and ferromagnetic single electron transistors consisting of ferromagnetic quantum dots.

The modeling of the spintronic devices utilized the advanced Green's function techniques, such as Keldysh Green's functions, which allowed accurate modeling by combining the quantum mechanically calculated electronic structure of the devices with the quantum statistical transport theory. This way the effects of scattering and collisional broadening of the energy levels could also be conveniently included in the models. The models predicted strongly spin-dependent transport and large changes in the magnetotransport properties of the spintronic semiconductor devices at temperatures close to the ferromagnetic ordering temperature or in moderate magnetic fields. The model for the ferromagnetic quantum dots predicted Kondo-like resonances in the conductance at high temperatures.

In the experimental part of the work the ferromagnetic thin films, pn-junctions, Esaki-Zener tunnel diodes, Schottky diodes, and resonant tunnelling diodes were fabricated using Molecular Beam Epitaxy technique for the growth of the Mn doped GaAs layers. The electrical and magnetic properties of these devices were studied by measuring the I-V characteristics, Hall effect, magnetoresistance, and magnetization as a function of temperature and magnetic field. The main result was the observation of the tunnelling anisotropic magnetoresistance effect (TAMR) in the Esaki-Zener tunnel diodes and the resonant tunnelling diodes. The effect was observed at very low bias voltages, which might allow the realization of ultra low-power spintronic devices. The developed models explained the measured magnetotransport properties. As an example, applying the spin-disorder scattering model a good quantitative agreement was obtained between the measured and calculated resistance and magnetoresistance in Mn doped GaAs layers in wide temperature and magnetic field ranges.

Tiivistelmä

Työssä tutkittiin teoreettisesti ja kokeellisesti voimakkaan vaihtovuorovaikutuksen, magneettisen järjestäytymisen, ja spin-fluktuaatioiden vaikutuksia spintroniikan puolijohdekomponenttien sähköisiin kuljetusominaisuuksiin. Oleellisena osana tutkittujen komponettien rakennetta oli magnaanilla seostettu GaAs-kerros tai ferromagneettinen kvanttipiste. Tutkittuja komponentteja olivat pn-liitokset, Schottky-diodit, spin Esaki-Zener-tunnelidiodit, resonanssitunnelidiodit, ja ferromagneettiseen kvantti-pisteeseen perustuvat yksielektroni-transistorit.

Komponenttien mallinnuksessa käytettiin Greenin funktiotekniikkaa, kuten Keldyshin Greenin funktioita, mikä mahdollisti tarkan kvanttistatistisen mallinnuksen, jossa otettiin huomioon mm. sironnan vaikutus kvanttimekaanisesti laskettujen energiatilojen leviämiseen. Mallit ennustivat voimakkaasti varauksenkuljettajien spinistä riippuvia kuljetusilmiöitä, kuten magnetoresistanssia ja spinistä riippuvaa tunneloitumista, erityiseti ferromagneetisen transitiopisteen läheisyydessä ja ulkoisen magneettikentän vaikuttaessa. Malli ferromagneettisille kvanttipisteille ennusti Kondo-tyyppistä konduktanssiresonanssia korkeissa lämpö-tiloissa.

Työn kokeellisessa osassa valmistettiin useita spintroniikan puolijohdekomponentteja kuten ferromagneettisia diodeja käyttäen Molekyylisuihku-tekniikkaa mangaanilla seostettujen GaAs-ohutkalvojen kasvatuksessa. Komponenttien sähköisiä ja magneettisia ominaisuuksia tutkittiin mittaamalla I-V ominaiskäyrät, Hall ilmiö, magnetoresistanssi ja magnetointi lämpötilan ja magneettikentän funktiona. Tärkein tulos oli epäisotrooppisen tunnelimagnetoresistanssi-ilmiön löytyminen Esaki-Zener-tunnelidiodeissa ja ferromagneettisissa resonanssitunnelidiodeissa. Ilmiö havaittiin myös hyvin pienillä jännitteillä, mikä periaatteessa mahdollistaa hyvin pienitehoisten spintroniikan komponenttien toteutuksen. Työssä kehitetyt teoreettiset mallit selittivät havaitut magnetosähköiset ilmiöt. Esimerkiksi spin-epäjärjestyssironnan malli kuvasi tarkasti Mn-seostetuissa GaAs-ohutkalvoissa mitatun resistiivisyyden ja magnetoresistanssin laajalla lämpötila-alueella ja kaikilla mittauksissa käytetyillä magneettikenttäarvoilla.

Preface

The research work for this doctoral dissertation was carried out in the Electron Physics Group in the Department of Micro and Nanosciences at the Aalto University School of Electrical Engineering (formerly Helsinki University of Technology). I wish to express my gratitude to my supervising professor, Professor Pekka Kuivalainen, for the opportunity to work in the group and for his advice and guidance in the modeling part of the work. The experimental part of the work was conducted under the supervision of Dr. Sergey Novikov. I am much obliged to him for his committed support and advice during the work.

The present thesis was a part of the projects "New semiconductor devices for spintronics" and "Room temperature spintronics" funded by the Academy of Finland during 2002-2007. Also the financial support from the Dean of the School of Electrical Engineering, Professor Tuija Pulkkinen, to finalize the thesis during 2012-2013 is appreciated.

I wish to thank all my co-authors for their contribution and pleasant collaboration. I am especially grateful to Dr. Heikki Holmberg for the joint journey to the world of accurate measurements at low temperatures. I wish to thank Professor Magnus Willander and Professor Jouni Ahopelto for pre-examing this dissertation and Professor Ronald Österbacka for agreeing to act as the opponent at the public examination of the dissertation. I also would like to thank Ms Charlotta Tuovinen for revising the language of my publications. In fact, I wish to express my gratitude to all my co-workers in the Electron Physics Group, but especially to Professor Hele Savin for the working opportunities and her support during the last few years.

Last, but not least, I am very grateful to my family, my husband Dmitry and my children Alexey and Ilia, for their love and support, encouragement and understanding throughout my studies.

Natalia Lebedeva

Espoo 16.3.2013

Contents

List of Publications

This thesis consists of an overview and the following publications which are referred to in the text by their Roman numerals.

I.   N. Lebedeva and P. Kuivalainen, Shift in the absorption edge due to exchange interaction in ferromagnetic semiconductors, Journal of Physics: Condensed Matter, vol. 14, pp. 4491-4501, 2002.

II.   N. Lebedeva and P. Kuivalainen, Modeling of ferromagnetic semiconductor devices for spintronics, Journal of Applied Physics, vol. 93, pp. 9845-9864, 2003.

III.   H. Holmberg, N. Lebedeva, S. Novikov, J. Ikonen, P. Kuivalainen, M. Malfait, and V. V. Moshchalkov, Large magnetoresistance in a ferromagnetic GaMnAs/GaAs Zener-diode, Europhysics Letters, vol. 71, pp. 811-816, 2005.

IV.   H. Holmberg, N. Lebedeva, S. Novikov, P. Kuivalainen, M. Malfait and V. V. Moshchalkov, Electrical transport in Mn-doped GaAs pn-diodes, Physica Status Solidi (a), vol. 204, pp. 791-804, 2007.

V.   H. Holmberg, G. Du, N. Lebedeva, S. Novikov, P. Kuivalainen and X. Han , Magnetotransport in ferromagnetic Schottky diodes made of Mn-doped GaAs, Journal of Physics: Conference Series, vol. 100, p. 052075, 2008.

VI.   H. Holmberg, N. Lebedeva, S. Novikov, M. Mattila, P. Kuivalainen, G. Du, X. Han, M. Malfait and V. V. Moshchalkov, Magnetotransport of holes through an AlAs/GaAs/AlAs resonant tunnelling quantum well with a ferromagnetic $Ga_{1-x}Mn_xAs$ emitter, Physica Status Solidi (a), vol. 204, pp. 3463-3477, 2007.

VII.   N. Lebedeva and P. Kuivalainen, Spin-dependent current through a ferromagnetic resonant tunnelling quantum well, Physica Status Solidi (b), vol.242, pp. 1660-1678, 2005.

VIII.   N. Lebedeva, H. Holmberg and P. Kuivalainen, Interplay between the exchange and Coulomb interactions in a ferromagnetic semiconductor quantum dot, Physical Review B, vol. 77, p. 245308, 2008.

Author's contribution

Publication I: The author has derived the equations of the model, written the computer code, analyzed the results and written the manuscript.

Publication II: The author has derived most of the equations of the model, written the computer code, and analyzed the results. The author also has written the first version of the manuscript.

Publication III: The author has grown the Mn doped GaAs samples together with Dr. Sergey Novikov, fabricated the tunnelling diodes, and participated actively the writing of the manuscript. The measurements of the *I-V* characteristics, and magnetoresistance were carried out together with Dr. Heikki Holmberg. The magnetization measurements were carried out by Dr. Mathias Malfait in Belgium.

Publication IV: The author has grown the Mn doped GaAs thin films, fabricated the diode structures, performed the measurements of the *I-V* characteristics and magnetoresistance together with Dr. Heikki Holmberg, and written the first version of the manuscript. She also performed the fitting of the models to the experimental results. The magnetization measurements were carried out by Dr. Mathias Malfait in Belgium.

Publication V: The author has grown the Mn doped GaAs thin films, fabricated the Schottky diodes and performed all the measurements together with Mr. Du. The author also has actively participated the writing of the manuscript.

Publication VI: The author has grown the Mn doped GaAs layers in the resonant tunnelling diodes, but the nonmagnetic AlAs layer were grown by Marco Mattila using MOVPE. The rest of the diode structures were fabricated by the author. The *I-V* characteristics were measured by the author together with Mr. Du. The author also analyzed the results, and wrote the first version of the manuscript.

Publication VII: The author has actively participated in the derivation of the model equations and in the writing of the computer code. The author has written the first version of the manuscript.

Publication VIII: The author has actively participated in the derivation of the model equations and in the writing of the computer code. The author has written the first version of the manuscript.

List of Abbreviations

DE	Double exchange (interaction)
DH-model	Dubson-Holcomb model
DMS	Diluted magnetic semiconductor
DOS	Density of states
EOM	Equation of motion (technique)
FRTD	Ferromagnetic resonant tunnelling diode
FSET	Ferromagnetic single electron transistor
FSQD	Ferromagnetic semiconductor quantum dot
GMR	Giant magnetoresistance effect
HH	Heavy hole
LH	Light hole
LT-MBE	Low temperature molecular beam epitaxy
MBE	Molecular beam epitaxy
MFA	Molecular field approximation
MIT	Metal-Insulator transition
MOCVD	Metal-organic chemical vapor deposition
MR	Magnetoresistance
MRAM	Magnetic random access memory
MTJ	Magnetic tunnel junction
QD	Quantum dot
QW	Quantum well
RHEED	Reflection high energy electron diffraction
RKKY	Ruderman-Kittel-Katsuya-Yoshida (interaction)
RTD	Resonant tunnelling diode
SRH theory	Shockley-Reed-Hall recombination theory
TAMR	Tunnelling anisotropic magnetoresistance
TMR	Tunnelling magnetoresistance

List of Symbols

a_0	Lattice constant
A	Area of a diode
B	Magnetic field
C	Constant
$D_c(E)$	Density of states for conduction band
$D_v(E)$	Density of states for valence band
$D_{n\sigma}$	Diffusion coefficient for spin-up or spin-down electrons
D_p	Diffusion coefficient for holes
E	Energy
$E_{c\sigma}$	Energy of the conduction band edge maximum (for spin-up and spin-down electrons)
$E_{v\sigma}$	Energy of the valence band edge minimum (for spin-up and spin-down holes)
ΔE_c	Conduction band offset in GaMnAs due to heavy doping
ΔE_v	Valence band offset in GaMnAs due to heavy doping
E_F	Fermi energy
E_m	Mobility edge
$f(E)$	Occupation probability
g_L	Landé factor
$\hbar$	Planck constant
H	Hamiltonian operator
I	Current
I_{tot}	Total current of a diode
I_{diff}	Diffusion current of a diode
I_{rec}	Recombination current of a diode
I_{tunn}	Tunnelling current of a diode
I_x	Excess tunnelling current of a diode (through defect states in bandgap)
J_{exch}	Exchange coupling parameter
J_{exch}^{sd}	Exchange coupling parameter for electrons
J_{exch}^{pd}	Exchange coupling parameter for holes

J_{exch}^{td}	Exchange coupling parameter for electrons on the impurity level
k_B	Boltzmann constant
$\mathbf{k}$	Wave vector of electron (hole)
$L_{n\sigma}$	Diffusion length for spin-up or spin-down electrons
L_p	Diffusion length for holes
m_0	Electron rest mass
$m_{e(h)}{}^*$	Effective mass of electron (hole)
n	Electron concentration
n_i	Intrinsic carrier concentration
N_A	Acceptor doping concentration
N_D	Donor doping concentration
N_c	Effective density of states for conduction band
N_v	Effective density of states for valence band
p	Hole concentration
q	Electron charge
R	Resistance
R_S	Series resistance
S	Spin quantum number of the magnetic atom
$\mathbf{S_R}$	Spin operator of a magnetic atom at the lattice site $\mathbf{R}$
$\mathbf{s}$	Spin operator of a charge carrier (electron or hole)
$\langle S^Z \rangle$	Thermal average of the spin polarization of magnetic atoms
$S_\sigma(E)$	The supply function (for spin up and spin down carriers)
T	Absolute temperature
T_c	Curie temperature
$T_\sigma(E)$	Tuneling probability (for spin up and spin down carriers)
V	Voltage
x	Mole fraction of magnetic atoms (Mn) in the host semiconductor (GaAs)
$\Delta_{1(2)}$	Band splitting parameter for conduction (valence) band in a ferromagnetic semiconductor

$\delta(x\text{-}x_0)$	Dirac's delta function
δ_{ij}	Kronecker's delta
μ_B	Bohr magneton
μ	Mobility
μ^{σ}_{tot}	Total mobility (for spin-up and spin-down carriers)
μ_{imp}	Mobility due to impurity scattering
μ^{σ}_{SD}	Mobility due to the spin-disorder scattering (for spin-up and spin-down carriers)
ρ	Resistivity
σ	Spin index ($\uparrow$ or $\downarrow$)
τ^{σ}	Relaxation time for excess charge carriers (for spin up and spin down carriers)
τ_{SD}^{σ}	Relaxation time for excess charge carriers related to the spin-disorder scattering

1 Introduction

Spintronics (short for "spin electronics"), also known as magnetoelectronics, is an emerging technology exploiting both the intrinsic spin of the electron and its associated magnetic moment, in addition to its elementary charge, in solid state devices. This relatively new field enriches conventional electronics with multifunctional devices that consume less energy, since the energy needed to change the orientation of spin is much smaller than the energy typically required in charge transport.[1]

Spintronics emerged from discoveries in the 1980s concerning spin-dependent electron transport phenomena in the solid-state devices. This includes the observation of spin-polarized electron injection from a ferromagnetic metal to a normal metal by Johnson and Silsbee [2] in 1985, and the discovery of giant magnetoresistance (GMR) independently by Albert Fert et al. [3] and Peter Grünberg et al. [4] in 1988. The GMR effect is related to a strong dependence of conductivity on the mutual magnetic orientation of two ferromagnetic layers separated by a non-magnetic metal layer. Nowadays GMR is widely utilized in read heads of computer hard drives and in magnetic field sensors. The origin of spintronics can be traced back even further to Mott's innovative concept of spin dependent conduction [5], ferromagnet/ superconductor tunnelling experiments pioneered by Meservey and Tedrow [6], and initial experiments on magnetic tunnel junctions by Julliere [7] in the 1970s suggesting a tunnelling magnetoresistance (TMR)-effect. TMR is utilized in the Magnetic Random Access Memories (MRAMs), which are based on magnetic tunnel junctions. [8]

So far all the commercial spintronic applications are based on magnetic metals. However, there are clear advantages when the metal thin films are replaced by magnetic semiconductors in spintronic applications. These advantages include, e.g., the following: (i) integration of spintronics with conventional semiconductor technology [8] , (ii) large magnetoresistance effects [9], (iii) the possibility to control the magnetic properties by charge injection and electric field in the case of carrier induced ferromagnetism[10], (iv) semiconductor-based spintronic devices could provide amplification and serve as multifunctional devices [10], (v) the possibility to fabricate magneto-optoelectronic devices [11], and (vi) the possibility to reach 100% spin polarization for charge carrier spins [12].

Semiconductor spintronics started from the research of the magnetic semiconductors such as Eu and Cr chalcogenides [9]. Later, due to difficulties in fabricating these materials and their low Curie temperatures (T_c < 100K), the interest shifted to diluted magnetic semiconductors (DMS), such as $Cd_{1-x}Mn_xTe$

and $Zn_{1-x}Mn_xTe$, where the magnetic properties can be controlled by altering the content of the magnetic Mn ions. [13-15]. These DMSs could be called the magnetic semiconductors of "the second generation" in contrast to the "first-generation" magnetic semiconductors such as Eu chalcogenides (EuO and EuS) and Cr-chalcogenide spinels ($CdCr_2Se_4$ and $CdCr_2S_4$). Later on DMSs based on III-V compounds such as $Ga_{1-x}Mn_xAs$ [16] and $In_{1-x}Mn_xAs$ [17] became a subject of intensive research because of their compatibility with conventional GaAs-based heterostructure technologies and subsequently because of their possible use in optoelectronic devices and integrated circuits. Moreover, $Ga_{1-x}Mn_xAs$ and $In_{1-x}Mn_xAs$ reveal ferromagnetic behavior, generally not observed in the II-VI or IV-VI DMSs. The first actual ferromagnetic DMS structure (Mn doped InAs film on top of GaAs substrate) was fabricated by Munekata's group in 1989 [18]. Recently many research groups have started to fabricate and study also actual spintronic devices such as Schottky diodes, p-n diodes, tunnelling diodes and resonant tunnelling diodes [19].

The main goal in the research of DMSs is to find materials suitable for room temperature applications, i.e., having Curie temperatures $T_c > 300K$. Though the highest T_c observed so far in GaMnAs is 185K [20], recently some high-T_c ferromagnetic semiconductors have been reported, such as Mn-doped $CdGeP_2$[21], Mn-doped GaN [22], GaP [23] and TiO_2 [24]. So, even if the attempts to raise Curie temperature in GaMnAs up to room temperature would not be successful, the experience obtained in the modeling and characterization of the GaMnAs-based devices can be useful in the design of the devices made of more suitable materials.

The present work contributes to the modeling, fabrication, and characterization of the spintronic semiconductor devices made of Mn doped GaAs. At the beginning of the thesis electronic properties and methods of preparation of Mn doped GaAs are briefly discussed. Then the theoretical estimates for the effect of ferromagnetism on electronic properties of GaMnAs are presented in chapter 3. The theory of basic semiconductor devices with a ferromagnetic GaMnAs layer is presented in chapter 4. For every device the most important experimental results are shown together with theoretical results for comparison. A summary of the results is given in chapter 5.

In Publication I, the effect of the strong exchange interaction on the shift of the band edges is calculated as a function of temperature and magnetic field in ferromagnetic semiconductors. The theoretical results are compared to exper-

imental ones both in Mn doped GaAs and in EuO, and a good agreement between the calculated and measured results is found.

In Publication II, the models for the basic semiconductor devices such as pn- and Schottky diodes and bipolar transistors, all having a ferromagnetic Mn doped GaAs layer, are developed and the model predictions are discussed.

Publications III and IV are the first ones, where the experimental *I-V* characteristics of the magnetic pn-diodes made of Mn doped GaAs are studied thoroughly. The most important result was the observation of a large spin-dependent tunnelling effect in the Esaki-Zener tunnelling diodes.

Publication V presents the experimental results on the first Schottky diode made of Mn doped GaAs. In Publications VI and VII the results from the experimental and theoretical studies of ferromagnetic resonant tunnelling diodes having a ferromagnetic Mn doped GaAs layer as a part of the device structure are discussed. The theory predicts that the largest spin-dependent effects are present in the case where the quantum well in the RTD structure is ferromagnetic, whereas in the experimental work only a ferromagnetic emitter could be fabricated. However, also in this case evidence of tunnelling anisotropy magnetoresistance (TAMR) effect was found in the measured *I-V* characteristics.

Finally, in Publication VIII, a ferromagnetic single-electron transistor (FSET) consisting of a ferromagnetic Mn doped GaAs quantum dot coupled to non-magnetic current leads is analyzed theoretically. The main result is the prediction that due to the spin disorder scattering in a FSET the conductance vs. gate voltage should show a Kondo-like behaviour at temperatures much higher than the Curie temperature.

2 Diluted magnetic semiconductors

2.1 General

Diluted magnetic semiconductors (DMS) is a class of semiconducting compounds based on conventional semiconductors, such as GaAs, in which a controlled fraction of non-magnetic cations is substituted by magnetic ions. The most common doping atom is Mn, but also Cr and Fe are widely used [25]. It is generally agreed that the ferromagnetic ordering in DMS is caused by the exchange interaction between magnetic impurities mediated by free electrons or holes[17,26]. This interaction is manifested, e.g., as strong temperature and magnetic field dependences of the optical and electrical properties of the magnetic semiconductors. For instance, below a Curie temperature or in high magnetic fields ferromagnetic semiconductors display a strong redshift in the fundamental optical absorption edge [27] and a band splitting when spin-up and spin-down sub-bands are formed.[28] Also, in the resistivity a prominent peak at the Curie temperature T_c has been found, which then disappears in sufficiently high magnetic fields, showing a large negative magnetoresistance (MR).[8,29,30]

2.2 Growth of GaMnAs thin films

GaMnAs is the most studied III-V DMS material so far. Ideally, the Mn ion substitutes a Ga atom in the GaAs lattice, closes a d-shell, acquiring a core spin S=5/2, and gives a hole to the system. The central open question regarding the origin of hole-mediated ferromagnetism in GaMnAs is if the carriers reside in the valence band of the host or if they form a narrow impurity band in the band gap. This characteristic of the carriers determines if the interaction is of Rudermann-Kittel-Katsuya-Yoshida (RKKY) or of double-exchange (DE) type. Evidences for both mechanisms have been claimed, making a consensus impossible. RKKY interaction[35,36] can be shortly described as follows: Mn spins have a strong antiferromagnetic kinetic exchange coupling J_{pd} with the hole spins; for metallic systems, the motion of holes mediates a ferromagnetic interaction between Mn ions leading to spontaneous magnetization. This would explain why ferromagnetism is found in GaMnAs even when the concentration x of the magnetic Mn ions is below the percolation threshold, and the direct (antiferromagnetic) coupling between the Mn ions is negligible.
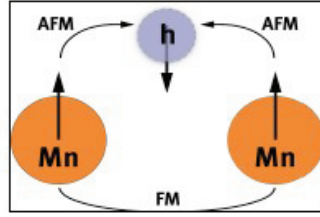
Figure1. *Sketch of the RKKY interaction. One Mn ion couples antiferromagnetically to an itinerant hole, which, in the next step, couples antiferromagnetically to the next Mn ion. Thus, both Mn ions couple ferromagnetically.*

The Zener-model[31,32] simplification of the RKKY theory is able to explain most of the properties of GaMnAs, still it has some drawbacks. While it assumes that holes mediating ferromagnetic coupling between far separated Mn atoms move in the unpertubed valence band of the host GaAs, there are experimental and theoretical evidences of degeneracy and Mn impurity band formation even at 1-2% doping level[33,34]. The position of the Fermi level inside the impurity band brings forth the hopping mechanism of ferromagnetism: the manganese 3d-electrons hop to the anion and further to the next Mn cation. In special configurations with two different Mn valences present (d^4-d^5 or d^5-d^6), this indirect exchange gives rise to ferromagnetic coupling. This model is known as the double exchange interaction (DE)[37,38].

Since ferromagnetism in GaMnAs is induced by holes, the onset of ferromagnetic ordering requires a certain hole concentration, and the Curie temperature T_c grows monotonically with the hole concentration p[8] . Transition metals as dopants exhibit a very low solubility ($x < 10^{18}$ cm^{-3}) in GaAs when bulk samples are grown by standard procedures such as Czochralski or Bridgman-Stockbarger[39]. Thus, in order to reach Mn concentrations in the percentage range, which are required for the occurrence of ferromagnetism, special non-equilibrium growth conditions have to be met. The method of choice for producing GaMnAs thin films is low-temperature molecular-beam epitaxy (LT-MBE). In conventional MBE, GaAs thin films are grown at substrate temperature somewhere in the range of 500-600°C on a GaAs bulk sample. By lowering the substrate temperature to around 240°C the co-evaporated Mn is not able to constantly remain at the surface of the substrate or form a second phase (MnAs), but is directly incorporated into the lattice[40]. However the low temperature and high As overpressure conditions result in a huge amount of defects already known from pure GaAs[41], most crucial among them are As-antisites (As$_{Ga}$). As$_{Ga}$ acts as a two level deep double donor and partly compensates Mn-induced hole carriers. Another important type of defects is Mn, in-

corporated into interstitial sites instead of Ga sites (Mn_{int}), which also acts as double donor and compensates the desired substitutional Mn (Mn_{sub}). Therefore the density of holes, p, is generally smaller than the density of the Mn ions in the LT-MBE grown GaMnAs.
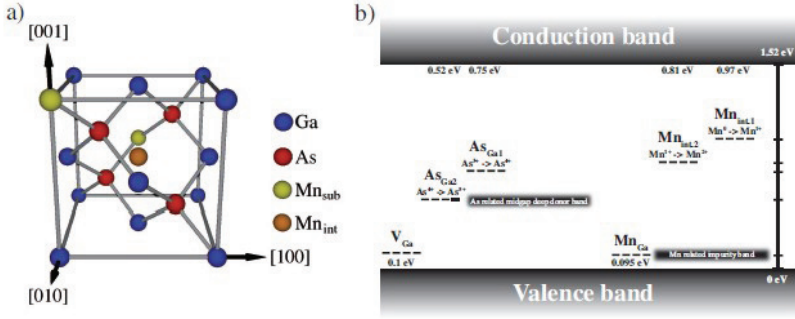

Figure.2 a) *Mn defect (Mn_{int}) in the crystal structure of GaMnAs, predetermined by GaAs host* ***b)*** *Location of the doping levels in the forbidden gap of GaAs: Mn on Ga-sites act as acceptor while both As on Ga-sites and Mn interstitial act as "deep" donors, partly compensating Mn acceptors.*

The effects of growth temperature and Mn content on the properties of the grown GaMnAs are best visualized in the GaMnAs phase diagram in Fig.3: there exists certain range of growth temperatures, where samples grow metallic; however both lightly and heavily doped samples grow insulating, first due to lack of charge carriers, second due to compensation.
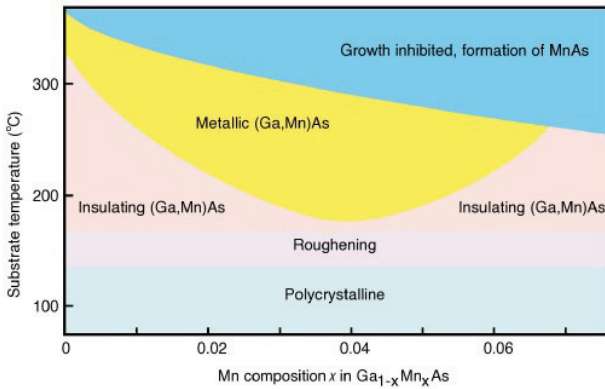

Figure 3. Phase diagram of GaMnAs. The sample properties depend crucially on the substrate temperature during growth and the Mn content. Homogeneous and metallic samples are desired. Adopted from ref.[42] Reprinted with permission from H.Ohno.,Science, vol. 281, p. 951-955, 1998. Copyright 1998, American Institute of Physics.

In the year 2002 it was shown[43] that annealing of the GaMnAs film subsequently to the growth results in a significant improvement of both magnetic and transport properties. The recipe consists of annealing the samples at moderate temperatures (typically 190°C), close to the growth temperature for comparable long durations (typically 100 h) in air. This procedure helps to remove Mn from interstitial positions, thus reducing compensation and increasing hole concentration (and consequently raising the Curie temperature).

All the Mn doped GaAs samples used in the experimental parts of the Publications III, IV, V, and VI were grown following the above ideas.

2.3 Energy band structure of GaMnAs

The energy band structure of GaMnAs around the band gap for various Mn concentrations can be deduced from that of GaAs and summarized in the following way [28,44,45]:

- The acceptor level related to Mn is positioned 110meV above the edge of the valence band.

- The excess As incorporated into the GaAs matrix during the LT-MBE growth is mainly in a form of arsenic antisites As_{Ga}, and As acts as a donor partly compensating the Mn acceptors.

- As the Mn content increases the Mn acceptor level transforms into the impurity band in the forbidden gap of GaAs. The Fermi level lies within this band due to compensation. Still, before the Mn content reaches a level of 1-2%, there is a gap between the impurity band and the valence band and the material exhibits semiconductor-like conductivity at low temperatures (see Publication IV).

- A further increase of the Mn content leads to an overlap between the impurity band and the valence band. When the Fermi level crosses the edge of the valence band, the material undergoes a metal-insulator transition (MIT) and starts to exhibit non-zero conductivity at 0 K. The further broadening of the impurity band leads to a mixing between the localized impurity states and the delocalized valence band states. Importantly, the ferromagnetic ordering in GaMnAs occurs on both the insulating and metallic side of the MIT, which points to a possibility that also the localized impurity states may contribute to the ferromagnetic interaction beween the Mn atoms.

- A splitting of the band edges and a formation of spin-up and spin-down subbands due to the ferromagnetic ordering are predicted by the theory (see below

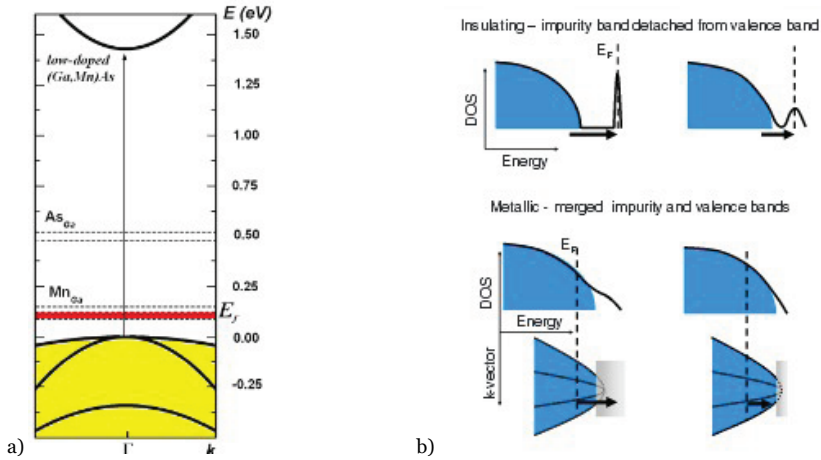and Publication I), and these effects have been observed experimentally in GaMnAs by means of magnetoabsorption [28].

Figure 4. (a) *Schematic energy band diagram for GaMnAs, splitting of the bands in the ferromagnetic state omitted for simplicity.* [44] ***(b)*** *Valence band density of states (DOS) evolution with increase of Mn content in GaMnAs.* [45] *Reprinted with permission from O. Yastrubchak Journal of Nano- and Electronic Physics Vol.4 No.1 p 01016, 1-6 (2012) and T.Jungwirth et al. Phys.Rev. B 76 125206, 1-9(2007) . Copyright 2007, American Institute of Physics.*

The schematic band diagram for GaMnAs shown in Figure 4 was used in the application of the Dubson-Holcomb-model in Publication IV (see also Ch. 3.2 below).

3 Modeling of the material parameters for GaMnAs thin films

In order to model semiconductor devices where a part of the device structure consists of the ferromagnetic GaMnAs layer we need to calculate the effect of the exchange interaction between the charge carrier spins and the spins of the localized magnetic electrons on the various material and device parameters such as the electronic states, recombination lifetimes and charge carrier mobilities. In this thesis the infinite-order perturbation theory based on Green's functions[46] was applied for these purposes. The retarded Green's function for the charge carriers interacting with the magnetic atoms was derived using an equation-of-motion (EOM) technique. The poles of the Green's function give the perturbed band energies and the band splittings caused by the magnetic ordering in GaMnAs. The relaxation time of the charge carriers due to spin disorder scattering was calculated from the imaginary part of the self-energy. Total mobility in the whole temperature range (0-300K) and in non-zero magnetic fields was calculated after taking into account the impurity scattering. The recombination lifetime for the minority carriers was calculated by introducing the band splitting into the standard theory for the direct and indirect (SRH) recombination. Here a summary of the theoretical results is presented, the details can be found in Publications I, II and IV.

3.1 Corrections to the band energies.

Strong exchange interaction between the charge carrier spins and the localized magnetic moments of Mn ions causes the so-called spin splitting of the energy levels of the charge carriers, i.e., the spin-up and spin-down sub-bands are formed. The energy difference between the spin-polarized sub-bands, the so-called band splitting parameter, is one of the most important parameters in the modeling of spintronic devices. Since the exchange interaction parameter J_{exch} for the holes is an order of magnitude larger than that for electrons, the shift of the valence band edge is more prominent than the shift of the conduction band edge.

In ferromagnetic semiconductors both the shift of the band edges and the band splitting parameter depend strongly on temperature and magnetic field. These effects have been experimentally observed, e.g., by studying the optical absorption in ferromagnetic semiconductors.[47] The dependence of the band edges on the magnetic order in a ferromagnetic semiconductor can be calculat-

ed using an infinite-order perturbation theory based on Green's functions (see Publications I and II). The total Hamiltonian describing the free carriers and the magnetic subsystem as well as their mutual interaction is given by:

$$H_{tot} = H_c^0 + H_{exch} + H_m \tag{1}$$

where $H_c^0 = \frac{\mathbf{p}^2}{2m^*}$ gives free carrier energies in the unperturbed band. The exchange term describes the exchange interaction between the free carrier spin $\mathbf{s}$ and the magnetic atom at a lattice point $\mathbf{R}$ having the total spin $\mathbf{S_R}$

$$H_{exch} = -\sum_{\mathbf{R}} J(\mathbf{r} - \mathbf{R}) \mathbf{s} \cdot \mathbf{S_R} \tag{2}$$

The exchange potential is assumed to be rapidly varying over the unit cell, $J(\mathbf{r} - \mathbf{R}) = J_{exch}\delta(\mathbf{r} - \mathbf{R})$, H_m is the Heisenberg Hamiltonian for the magnetic subsystem :

$$H_m = -\sum_{\mathbf{R},\mathbf{R'}} I(\mathbf{R},\mathbf{R'})\mathbf{S_R} \cdot \mathbf{S_{R'}} - g_L\mu_B B \sum_{\mathbf{R}} S_{\mathbf{R}}^Z \tag{3}$$

where the first term describes the magnetic coupling between the localized spins and the second term gives the Zeeman energy when an external magnetic field B is applied in the z-direction. After expressing the total Hamiltonian (1) using the second quantization formalism, it is a straightforward task to write down and solve the equation of motion for the Green's function of the charge carriers (Publications I,II, and IV). The final result is given by:

$$G_\sigma(\mathbf{k}, E) = (E - E_{\mathbf{k}\sigma}^{(1)} - \Sigma_\sigma^{(2)}(\mathbf{k}, E))^{-1} \tag{4}$$

where

$$E_{\mathbf{k}\sigma}^{(1)} = \frac{\hbar^2\mathbf{k}^2}{2m^*} - \frac{\Delta}{2}(\delta_{\sigma\uparrow} - \delta_{\sigma\downarrow}) \tag{5}$$

gives the first-order correction to the band edge, i.e., the splitting between spin-up and spin-down sub bands, $\Delta = xJ_{exch}\langle S^Z \rangle$. Here x is a mole fraction of magnetic ions, and $\langle S^Z \rangle$ is the average spin polarization of magnetic subsystem. The second order self-energy in (4) is given by:

$$\Sigma_\sigma^{(2)}(\mathbf{k}, E) = \frac{J_{exch}^2}{4N} \sum_{\mathbf{q}} \left[\frac{\Gamma^{xx}(\mathbf{q})\delta_{\sigma\uparrow}}{E - E_{\mathbf{k}-\mathbf{q},\downarrow}^{(1)}} + \frac{\Gamma^{yy}(\mathbf{q})\delta_{\sigma\downarrow}}{E - E_{\mathbf{k}-\mathbf{q},\uparrow}^{(1)}} + \frac{\Gamma^{zz}(\mathbf{q})}{E - E_{\mathbf{k}-\mathbf{q},\sigma}^{(1)}} \right] \tag{6}$$

where $\Gamma^{\alpha\alpha}(\mathbf{q})$ is the Fourier transform of the spin-correlation function. In the molecular field approximation (MFA) the average spin polarization of the magnetic moments and the spin-correlation functions can be calculated using the Brillouin function (see Publications I and II).

The results (4)-(6) are essential in the modeling of the material and device parameters for Mn doped GaAs, since the real part of the self-energy (6) gives

the higher order correction to the band energies, and its imaginary part gives an estimate for the relaxation time of the charge carries in the case of the spin-disorder scattering (see below).

The band splitting can be calculated self-consistently from Eqs. (4)-(6) by determining the poles of the Green's function (4) using numerical iterations as a function of temperature in various magnetic fields. In the case of GaMnAs we have used the following parameters: $S = 5/2$, $a_0 = 5.65$Å, the exchange integral for the holes $J_{exch}^{pd} = 1.4$eV, and the exchange integral for the electrons $J_{exch}^{sd} = 0.2$eV[28,29]. Curie temperature T_c is proportional to x, i.e., the fraction of magnetically active Mn ions, and can be estimated from the measured resistivity, Hall effect (see Publication IV), or it can be taken from literature [42].
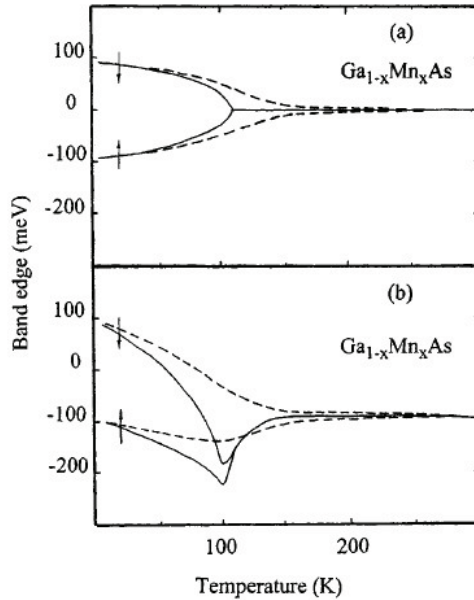
Figure 5. *Temperature dependence of the valence band edge in GaMnAs at B=0 (solid curves) and B=4T (dashed curves) showing the band splitting at Tc =110K: a) the first order result, b) the higher order result. Reprinted with permission from N. Lebedeva and P. Kuivalainen, Journal of Applied Physics, vol. 93, pp. 9845-9864, 2003. Copyright 2003, Americal Institute of Physics.*

Figure 5 shows the calculated temperature dependence of the valence band edge in GaMnAs as a function of temperature at two values of the magnetic field B. Higher-order corrections result in a 100 meV blue shift of the valence band edge already in the paramagnetic region $T > T_c$. This shift has been observed experimentally in a Gd-doped ferromagnetic semiconductor EuO (n-type)[47] as a red shift of the optical absorption edge, but not in the GaMnAs,

where it probably is screened by the bandgap narrowing due to eavy doping. In the present thesis only the first-order corrections, expressed by Eq. (5), to the valence and conduction band edges were taken into account in the modeling of semiconductor devices having a ferromagnetic GaMnAs layer.

Since the device structures considered in the present work typically consist of a heterojunction between a nonmagnetic (GaAs) and a magnetic (GaMnAs) material, a possible band discontinuity must be taken into account. In GaMnAs the bandgap narrowing due to a heavy p-doping is assumed and the energies for the conduction and valence band edges can be written as:

$$E_{c\sigma} = E_c^0 - \Delta E_c^0 - \frac{\Delta_1}{2}(\delta_{\sigma\uparrow} - \delta_{\sigma\downarrow}) \qquad (7)$$

$$E_{v\sigma} = E_v^0 + \Delta E_v^0 - \frac{\Delta_2}{2}(\delta_{\sigma\uparrow} - \delta_{\sigma\downarrow}) \qquad (8)$$

where the band splitting parameter $\Delta_1 = xJ_{exch}^{sd}\langle S^Z \rangle$ is for the conduction electrons and $\Delta_2 = xJ_{exch}^{pd}\langle S^Z \rangle$ for the holes. The conduction and valence band offsets were taken from literature [10,11] as $\Delta E_c^0 = 0.01eV, \Delta E_v^0 = 0.1e$.

3.2 Charge carrier mobility and recombination

Magnetic ordering in ferromagnetic semiconductors has two effects on charge transport:

- a resistivity peak at the Curie temperature T_c,
- a large negative magnetoresistance (MR) below T_c vanishing at temperatures well above T_c

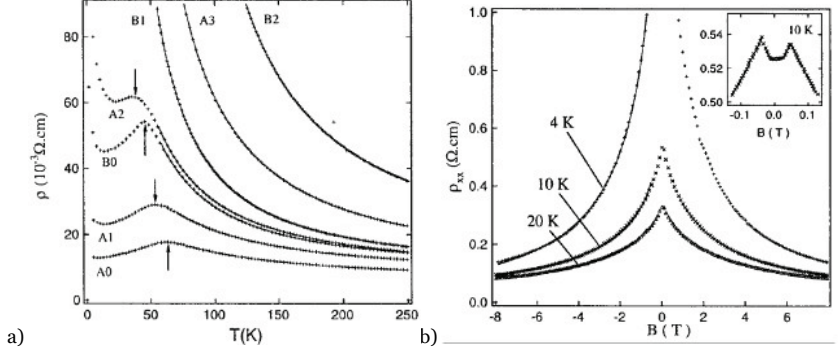Both these effects have been observed experimentally also in GaMnAs, as shown in Fig.6. [30]

Figure 6. (a) *Resistivity versus temperature for GaMnAs layers with differ-ent Mn content, arrows point to Curie temperature. Samples A0 and A1 are de-generate (metallic), B0 and A2 non-degenerate, though ferromagnetic, samples B1,B2 and A3 contain too little Mn for the onset of ferromagnetism.* **b)** *Resistivi-ty versus magnetic field at T< T_c for ferromagnetic GaMnAs layer. Reprinted with permission from A. Van Esch, L. Van Bockstal, J De Boeck et al Phys.Rev.B* **56**, *13103-13112 (1997) . Copyright 1997, American Institute of Physics. We have obtained similar results (see below and Publication IV).*

The resistivity peak and the large magnetoresistance can be explained as a contribution of the spin disorder scattering to the total mobility in ferromag-netic semiconductors. In order to evaluate this effect the abovementioned Green's function technique can be applied. An estimate for the relaxation time of the charge carriers $\tau_{SD}^{\sigma}(\vec{k})$ can be obtained from the imaginary part of the self-energy(6):

$$\frac{1}{\tau_{SD}^{\sigma}(\mathbf{k})} = \frac{2}{\hbar}\left|\text{Im}\Sigma_{\sigma}^{(2)}(\mathbf{k})\right| = \frac{2\pi}{\hbar}\left(\frac{J_{exch}^2}{4N}\right)\sum_{\mathbf{q}}\left[\Gamma^{xx}(\mathbf{q})\delta\left(E_{\mathbf{k}\sigma} - E_{\mathbf{k-q},\downarrow}\right)\delta_{\sigma\uparrow} + \right.$$
$$\left.\Gamma^{yy}(\mathbf{q})\delta\left(E_{\mathbf{k}\sigma} - E_{\mathbf{k-q},\uparrow}\right)\delta_{\sigma\downarrow} + \Gamma^{xx}(\mathbf{q})\delta\left(E_{\mathbf{k}\sigma} - E_{\mathbf{k-q},\sigma}\right)\right] \qquad (9)$$

In the degenerate semiconductor the charge carrier mobility can be estimated using Eq.(9) and the following simple expression:

$$\mu = \frac{q\tau(\mathbf{k_F})}{m^*} \qquad (10)$$

In the non-degenerated case $\tau(k_F)$ should be replaced by

$$\langle\tau\rangle = \frac{\int_0^\infty E^{3/2}e^{-(E-E_F)/k_BT}\tau(E)dE}{\int_0^\infty E^{3/2}e^{-(E-E_F)/k_BT}dE} \qquad (11)$$

Finally, in the presence of impurity scattering the total mobility can be calcu-lated according to Mathiessen's rule, which can be written as:

$$\frac{1}{\mu_{tot}^{\sigma}} = \frac{1}{\mu_{imp}} + \frac{1}{\mu_{SD}^{\sigma}} \qquad (12)$$

In order to explain the temperature dependence of resistivity in the whole temperature range 0-300 K and also in the case of low Mn concentration, a conduction mechanism related to the impurity states shown in Fig.2 must be added to the above resistivity model. This can be done with a Dubson-Holcomb (DH)-model [48] for resistivity in heavily doped semiconductors. In this model the temperature dependence of the resistivity is given by:

$$\rho_{DH}(T) = \rho_{300K} \left(\frac{300K}{T}\right) \left\{ \ln\left[1 + \exp\left(\frac{E_m - E_F}{k_B T}\right)\right]\right\}^{-1} \tag{13}$$

where E_m is the mobility edge in a disordered semiconductor.

Figure 7 shows the mobility vs. temperature in GaMnAs as calculated using Eqs. (9) and (10). The calculated hole mobility vs. temperature and magnetic field explains both the resistivity peak at the Curie temperature and negative magnetoresistance for $T < T_c$ (a detailed comparison of the resistivity model to the experimental results is done in Figure 11 in Ch. 4.1.2 below).
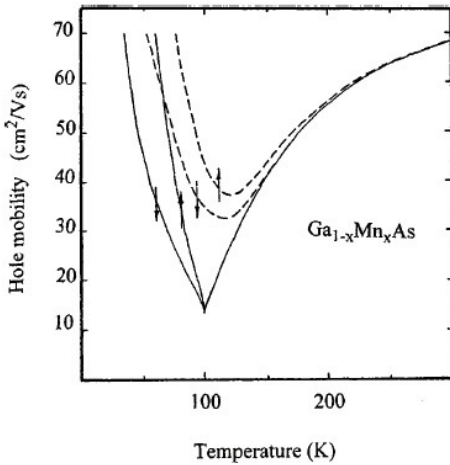
Figure 7. *Hole mobility vs. temperature for spin-up and spin-down carriers at B=0T (solid curves) and B=4T (dashed curves) in GaMnAs in the case of spin disorder scattering. The material parameters are the same as in Figure 5. Reprinted with permission from N. Lebedeva and P. Kuivalainen, Journal of Applied Physics, vol. 93, pp. 9845-9864, 2003. Copyright 2003, Americal Institute of Physics.*

The mobility is an important model parameter also in semiconductor devices, where the operation is based on charge carrier diffusion, such as pn-junctions and bipolar transistors. This is due to the fact that the diffusion coefficient of the charge carriers is proportional to the total mobility. In addition, in the pn-junctions and bipolar transistors minority carrier recombination plays an important role. The effects of the exchange interaction and band spiltting on

the recombination processes in a magnetic semiconductor have been discussed in Publication II. The model predicts, e.g., a strong magnetic field dependence for the recombination times, as shown in Figure 8. However, so far there is no experimental evidence for the spin dependence of the recombination processes in GaMnAs. This is due to the heavy doping concentration needed in the ferromagnetic samples, which strongly decreases the minority carrier life-time in Mn doped GaAs making it difficult to measure.
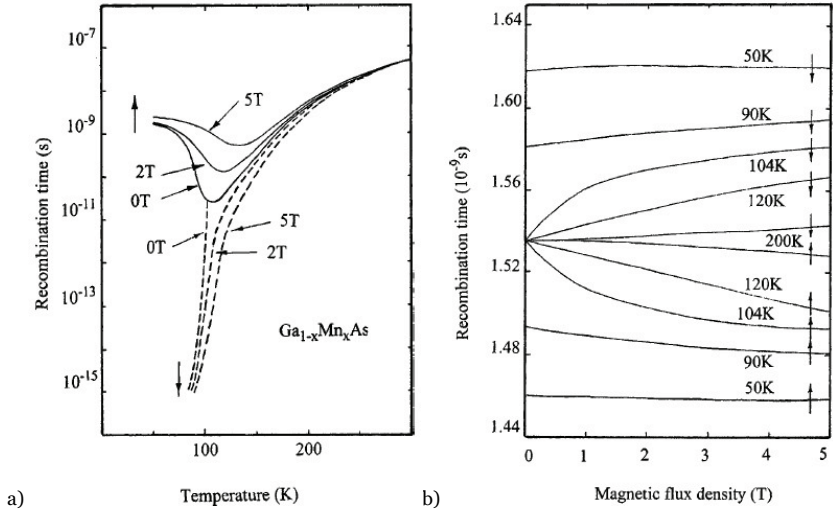

Figure 8. *Direct band-to-band recombination time vs. temperature and magnetic field in **a)** non-degenerate GaMnAs and **b)** degenerate GaMnAs. Reprinted with permission from N. Lebedeva and P. Kuivalainen, Journal of Applied Physics, vol. 93, pp. 9845-9864, 2003. Copyright 2003, Americal Institute of Physics.*

4 Semiconductor devices with a GaMnAs layer: theoretical modeling vs. experiments

4.1 Schottky diode

4.1.1 Modeling

The most simple semiconductor device is a Schottky diode consisting of a junction between a metal and a semiconductor. Since the current through the Schottky diode depends exponentially on the height of the potential barrier between the semiconductor and the metal, which in turn depends on the energy difference between the metal work function and the semiconductor band edge, the band splitting due to ferromagnetic ordering in a magnetic semiconductor should strongly affect the *I-V* curves of the diode. Thus, in principle, the ferromagnetic Schottky diode can be used as a sensitive magnetic field sensor. More generally, since the contact between the metal and the ferromagnetic semiconductor exists in all spintronic devices, the modeling of its characteristics as a function of temperature and magnetic field is a necessary task in the design of all spintronic semiconductor devices.

For simplicity we can start the modeling with a textbook example of a junction between an n-type magnetic semiconductor, such as Eu-chalcogenides, and a nonmagnetic metal having the work function larger than the electron affinity of the semiconductor. In the case of the junction between a p-type GaMnAs and the metal the band diagram should be just inverted.
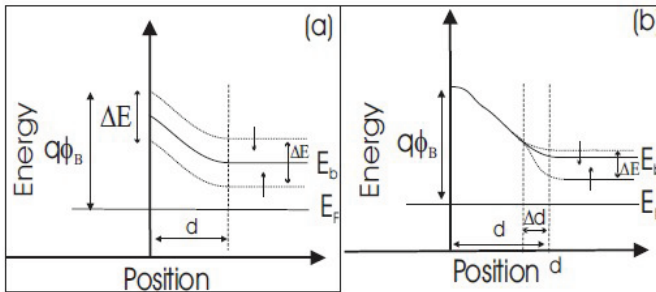

Figure 9. Energy band diagram for a ferromagnetic Schottky diode: (a) the ferromagnetic region extends into the depletion region having the width d, and (b) ferromagnetism is carrier induced, so that the magnetic layer extends only slightly into the depletion region. Reprinted with permission from H. Holmberg, G. Du, N. Lebedeva, S. Novikov, P. Kuivalainen, and X. Han, Journal of Physics: Conference Series, vol. 100, p. 052075, 2008. Copyright 2008, IOP Publishing Ltd.

Since in GaMnAs ferromagnetism is hole-induced, the situation depicted in Figure 9(b) is more realistic than that of Figure 9 (a). In Publication II the standard thermionic emission theory [49] was applied to the junction shown in Figure 9 (a), by taking into account the magnetization dependence of the conduction band edge. Total thermionic current in this case is given by:

$$I_{tot} \sim T^2 e^{\frac{-q\phi_B}{kT}} \cosh\left(\frac{\Delta E}{2k_BT}\right)\left(e^{\frac{qV}{kT}} - 1\right) \tag{14}$$

where the effect of magnetoresistance in the semiconductor layer on the voltage distribution over the diode structure can be taken into account by replacing V by $V - IR_S$. A negative magnetoresistance in the ferromagnetic semiconductor layer is assumed to cause a shift in the I-V curves towards lower voltages. If the band splitting is large enough($\Delta E \gg k_BT$), the model predicts a strong increase in the current through the Schottky diode after the onset of ferromagnetism, as shown in Figure 10. The negative magnetoresistance is expected to have a maximum in the vicinity of the T_c.
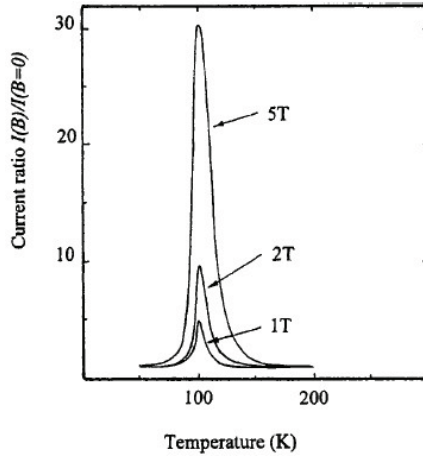

Figure 10. *Current ratio I(B)/I(B=0) vs. temperature in various magnetic fields in a ferromagnetic Schottky diode as calculated for the band diagram shown in Figure 9(a). Reprinted with permission from N. Lebedeva and P. Kuivalainen, Journal of Applied Physics, vol. 93, pp. 9845-9864, 2003. Copyright 2003, Americal Institute of Physics.*

There are experimental results for a Schottky diode made of a ferromagnetic n-type semiconductor EuCdS [50], as discussed in Publication II. The measured I-V characteristics followed Eq.(14), and an estimate for the barrier lowering (0.24 eV) could be made, which was in agreement with the result obtained from optical absorption measurements. The experimental results on Mn doped GaAs will be presented below in Ch. 4.1.2.(see also Publication V).

In the case of Figure 9(b) the thermionic component of the current remains unchanged under the onset of the band splitting. However, the tunnelling current increases due to a shortening of the barrier by Δ d. Since the tunnelling current depends exponentially on the barrier height $q\phi_B$ and the width d, the relative change of the tunnelling current due to band splitting can be written as

$$\Delta I/I \sim \exp\left(\Delta d\sqrt{\frac{2m^*q\phi_B}{\hbar^2}}\right) - 1 \tag{15}$$

where the shortening of the barrier can be estimated to be $\frac{\Delta d}{d} \approx \Delta E/q\phi_B$. Also in this case a negative magnetoresistance is expected in the Schottky diode, which, however, is much smaller than in the previous case.

4.1.2 Experimental result on Pt/GaMnAs Schottky diode

Various GaMnAs thin films with Mn mole fraction x varying from 0.02 to 0.05 were grown in our VG100H MBE system at Aalto University. All films were grown on semi-insulating GaAs (100) substrates. First, the surface was chemically cleaned and possible oxide was removed. After that a buffer layer of un-doped GaAs was grown at 580°C. Then the growth temperature was decreased to 230°C and a 1μm thick Mn doped GaAs layer was grown. During the growth process the crystalline quality of the film was controlled using a Reflection High Energy Electron Diffraction (RHEED)-technique. The Mn doped GaAs films were first characterized by measuring the resistivity vs. temperature. The ohmic contacts Pt/Ni/Pt/Au to the p+ layer were deposited by an e-beam vacuum evaporation technique and resistivity was measured in the Van-der-Pauw configuration. The hole concentration was evaluated at the room temperature through Hall measurements. The behavior of the resistivity curve changes from insulating to metallic while the hole concentration increases, as shown in Figure 11. These results are very similar to those obtained by another research group (see Figure 6 above). The onset of ferromagnetism is manifested by the appearance of a local maximum at T_c on the $\rho(T)$ curve. Negative magnetoresistance is seen in both magnetic field polarities, being most prominent at the Curie temperature (Figure 11b). The solid curves in Figure 11a have been calculated by combining the spin disorder scattering model, Eq.(9), with the Dubson-Holcomb-model, Eq.(13). The agreement between the theoretical and experimental results is excellent.
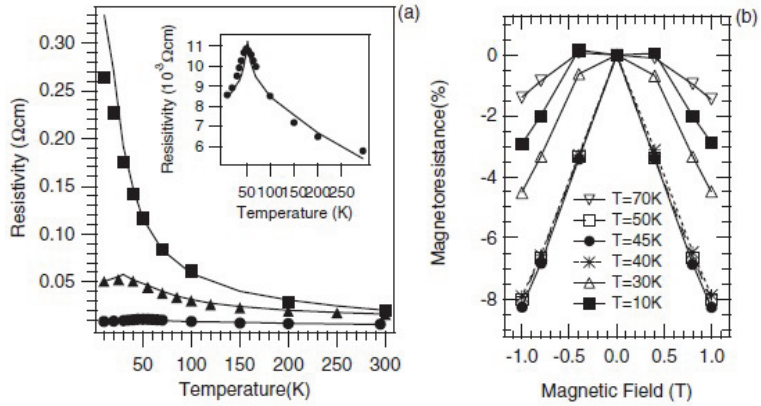
Figure 11. a) *Resistivity vs. temperature in GaMnAs films with room temperature hole concentrations 5.6 10^{19} ,7.0 10^{19} and 1.7 10^{20} cm^{-3}(from top to bottom); the inset shows the lowest curve in more detail. The solid curves have been calculated by combining the spin disorder scattering model, Eq. (7), with a Dubson-Holcomb model, Eq.(11).* **b)** *Magnetoresistance [ρ(B)- ρ(0)]/ ρ(0) vs. magnetic field at various temperatures in GaMnAs with x=0.04 (p=1.7 1020). Reprinted with permission from H. Holmberg, N. Lebedeva, S. Novikov, P. Kuivalainen, M. Malfait, and V. V. Moshchalkov, Physica Status Solidi (a), vol. 204, pp.791-804, 2007. Copyright 2007, WILEY-VCH Verlag.*

The ferromagnetic behavior of our GaMnAs samples with Curie temperatures varying from 30 to 70K was verified by direct magnetization measurements, an example is shown in Figure 12.
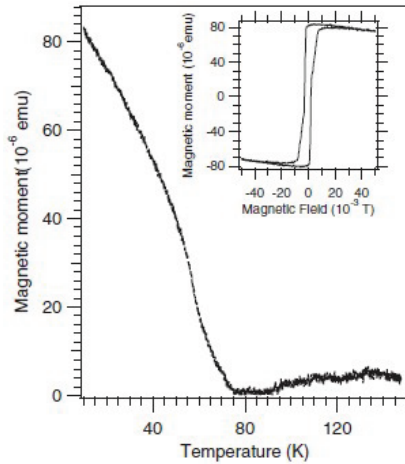
Figure 12. *Magnetic moment vs. temperature in a GaMnAs film measured by using a vibrating sample magnetometer at B=10mT. The inset shows the magnetic hysteresis measured at 10K. Reprinted with permission from H. Holmberg, N. Lebedeva, S. Novikov, P. Kuivalainen, M. Malfait, and V. V. Moshchalkov, Physica Status Solidi (a), vol. 204, pp.791-804, 2007. Copyright 2007, WILEY-VCH Verlag.*

The Schottky diode contacts on top of the GaMnAs layer were made of Pt metal using e-beam evaporation, the ohmic contacts on the backside were made of an Au/Ge/Ni alloy. For comparison also a non-magnetic GaAs Schottky diode was fabricated, where, instead of Mn doping, Be was used as a p-type dopant. The *I-V* curves for both diodes were measured at various temperatures (300-8K), without a magnetic field and in a magnetic field *B*=1T applied perpendicular to the plane of the device. The rectifying properties of the diodes are clearly seen regardless of the relatively low barrier between the Pt metal and heavily doped p-type GaAs, as shown in Figure 13.
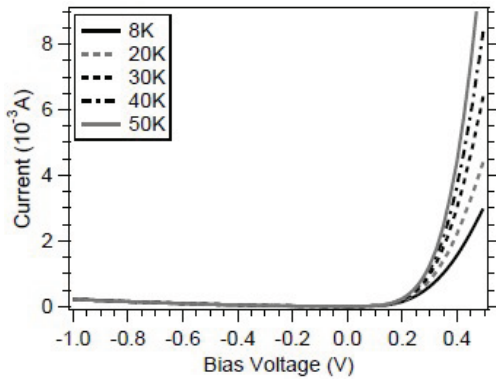
Figure 13. *Measured I-V curves of a magnetic Pt/GaMnAs Schottky diode at various temperatures (B=0T). Reprinted with permission from H. Holmberg, G. Du, N. Lebedeva, S. Novikov, P. Kuivalainen, and X. Han, Journal of Physics: Conference Series, vol. 100, p. 052075, 2008. Copyright 2008, IOP Publishing Ltd.*

A large negative magnetoresistance of about 30% at *T*=8K was observed in the magnetic diode, as shown in Figure 14, but not in the non-magnetic diode. The measured effect of the magnetic field on the current could be explained using a simple series resistance model, as shown in Figure 14a. In this model the contribution from the spin dependent tunnelling, Eq.(15), was kept independent of the magnetic field, and the only magnetic field-dependent contribution was assumed to follow from the magnetoresistance of the series resistance related to the Mn doped GaAs layer, as already shown in Figure 11.
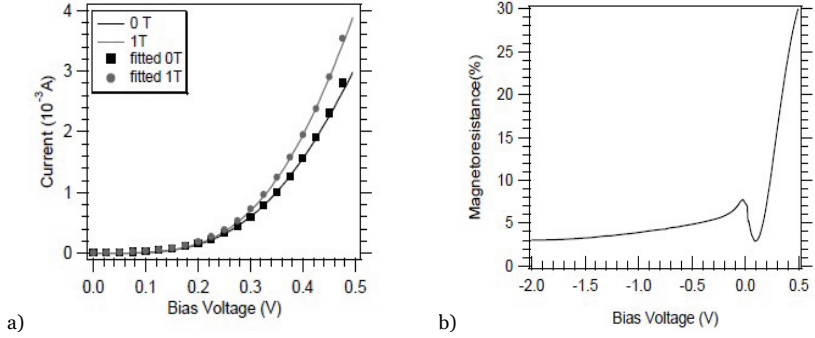
Figure 14. a) *Effect of the external magnetic field on the I-V curves of the magnetic Schottky diode at T=8K, dots show fitted curves calculated using a series resistance model.* **b)** *Magnetoresistance vs. bias voltage at T=8K. Reprinted with permission from H. Holmberg, G. Du, N. Lebedeva, S. Novikov, P. Kuivalainen, and X. Han, Journal of Physics: Conference Series, vol. 100, p. 052075, 2008. Copyright 2008, IOP Publishing Ltd.*

The only manifestation of the magnetization dependent tunnelling current may be the anomalous voltage dependent MR shown in Fig. 14b at low voltages. This effect may be related to a change from a tunnelling current dominating MR at low voltages to the series resistance dominated MR at higher voltages. However, this question remains open to some extent.

4.1.3 Conclusions

It is very straightforward to model the special properties of magnetic Schottky diodes by starting with the conventional thermionic emission theory and then adding the magnetization dependent effects by considering the band splitting and the consequent Schottky barrier lowering, and the magnetoresistance of the series resistance of the magnetic semiconductor layer. Our experimental results on Pt/GaMnAs Schottky diodes indicate the situation where the magnetic field-dependence of the series resistance masks the possible spin-dependent tunnelling contributions in the *I-V* characteristics.

Mn doped GaAs is not an optimal material for large magnetoresistance effects, since it is always of p-type leading to small Schottky barriers, and its Curie temperature is low allowing the appearance of significant MR effects only at low temperatures. A better candidate for sensitive magnetic field sensors would be, e.g., Mn doped GaN, which in addition to having a high T_c also has been reported to be of n-type. [51]

4.2 P-N diode

4.2.1 Modeling

As compared to the theoretical treatment of the Schottky diode, it is a much more difficult task to model a ferromagnetic p-n junction, since the operation of the p-n junction is based on the diffusion of the minority carriers and on the recombination processes discussed above. A possible energy band diagram for the junction between a p-type GaMnAs and nonmagnetic n-type GaAs is shown in Fig.15, where it is assumed that also the depletion region on the p-side of the diode is ferromagnetic.
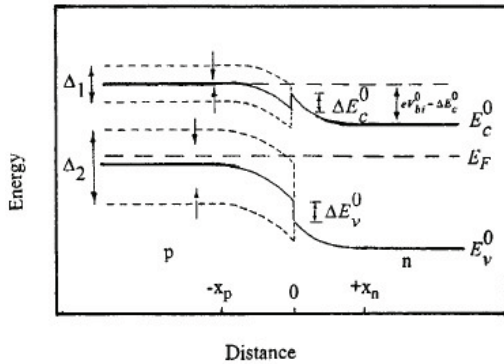
Figure 15. *Energy band diagram for a p-n junction between a ferromagnetic p-type and a nonmagnetic n-type semiconductor. Dashed curves show the spin-polarized band edges. Band gap shrinkage of the p-side due to heavy doping is taken into account through the conduction and valence band offsets ΔE_c and ΔE_v. Reprinted with permission from N. Lebedeva and P. Kuivalainen, Journal of Applied Physics, vol. 93, pp. 9845-9864, 2003. Copyright 2003, Americal Institute of Physics.*

A detailed theory of magnetic p-n diodes has been published in Publication II. Here we present a brief summary of the main results of the modeling. The total current of a magnetic p-n diode is given by:

$$I_{tot} = I_{diff} + I_{rec} + I_{tunn} + I_X \tag{16}$$

where I_{diff} is the diffusion current, I_{rec} is associated with the recombination processes in the depletion region, I_{tunn} is the tunnelling current associated with the direct band-to-band tunnelling through the depletion region, and I_X is the excess tunnelling current through defect states in the band gap.

Applying the ordinary Shockley theory of the p-n junction one can see that the diffusion component of the total current is affected by the conduction band splitting only:

$$I_{diff=} = Aqn_i^2 \left[\frac{D_{n\uparrow} e^{\frac{\Delta_1}{2kT} + \Delta E_c^0/kT}}{2L_{n\uparrow}N_A} + \frac{D_{n\downarrow} e^{\frac{\Delta_1}{2kT} + \Delta E_c^0/kT}}{2L_{n\downarrow}N_A} + \frac{D_p e^{-\Delta E_v^0/2kT}}{L_p N_D} \right] \left(e^{(qV - IR_S)/kT} - 1 \right) \quad (17)$$

where A is the area of the diode, n_i is the intrinsic carrier concentration, $D_{n\uparrow(\downarrow)}(D_p)$ is the carrier diffusion coefficient for the electrons (holes), $L_{n\uparrow(\downarrow)}(L_p)$ is the diffusion length of the electrons (holes), and $N_A(N_D)$ is the acceptor (donor) concentration, R_S is the series resistance of the diode. In the nonmagnetic case $\Delta_1 = 0$ and in the absence of the band discontinuities Eq.(17) reduces to the standard Shockley equation for a p-n junction. [49]

The magnetic part (the first two terms in Eq.(17)) will contribute significantly to the total current if the following condition is fulfilled:

$$N_D \geq N_A \sqrt{\frac{\tau_n D_p}{\tau_p D_n}} e^{-(\Delta E_c^0 + \Delta E_v^0)/kT} \quad (18)$$

In a GaMnAs p+n junction $N_A \gg N_D$, but the large band discontinuity in the valence band may help to reach the condition (18), and then a significant magnetoresistance effect is possible near the Curie temperature in the case depicted in Figure 15. Figure 16 shows the diffusion current vs. temperature in various magnetic fields as calculated from Eq.(17). The rather small magnetoresistance at low fields is due to the small value of the band splitting parameter Δ_1 in the conduction band of GaMnAs.
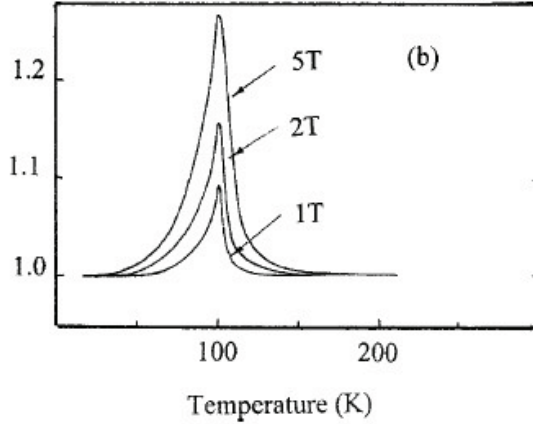

Figure 16. *Calculated diffusion current ratio I(B)/I(0) vs. temperature in various magnetic fields in an ideal ferromagnetic p-n junction. The results have been calculated from Eq.(17) with $\Delta_1=0.025eV$, $\Delta_2=0.1$ eV, $N_A/N_D=10$, and $T_C=100$ K. Reprinted with permission from N. Lebedeva and P. Kuivalainen, Journal of Applied Physics, vol. 93, pp. 9845-9864, 2003. Copyright 2003, Americal Institute of Physics.*

In Publication II we have shown that under favorable conditions, e.g., in magnetic p-n junctions with nondegenerate p- and n-regions, the magnetoresistance due to the recombination current may be even larger than the one related to the diffusion current. However, in GaMnAs p-n diodes the magnetic side is always heavily doped, which significantly reduces the MR effect, as discussed below.

4.2.2 Experimental results for GaMnAs p-n diodes with a lightly doped n-region

After the fabrication process for the ferromagnetic GaMnAs thin films was optimized, we started to fabricate p-n diodes having a GaMnAs layer as the p-side. The structure of the diode is presented in Figure 17. The doping concentration of the n-type substrate was $10^{17} cm^{-3}$, on top of which a 250 nm thick Si-doped GaAs film was grown ($n=10^{17} cm^{-3}$). Above the n-layer a 0.5μm thick GaMnAs p-layer was grown. Pt/Ni/Pt/Au and Au/Ge/Ni/Au ohmic contacts were evaporated on the front and back sides, respectively.
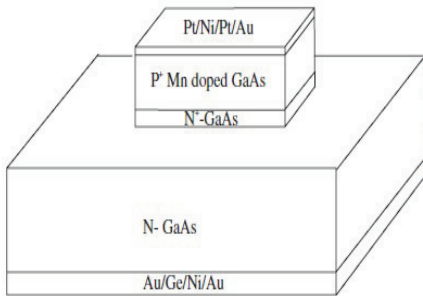
Figure 17*. Schematic structure of the magnetic p−GaMnAs/n-GaAs diode. Reprinted with permission from H. Holmberg, N. Lebedeva, S. Novikov, P. Kuivalainen, M. Malfait, and V. V. Moshchalkov, Physica Status Solidi (a), vol. 204, pp.791-804, 2007. Copyright 2007, WILEY-VCH Verlag.*

The I-V characteristics of the p-n diode were measured in the wide temperature range (10-300K), with and without a magnetic field perpendicular to the plane of the device ($B=\pm 1T$). The strong T-dependence of the I-V curves vanishes at T<100K, as shown in Figure 18. This behavior, which is similar to one reported by Arata et al. [11], can be attributed to the valence band offset between GaMnAs and GaAs: at low temperatures the T-dependent diffusion current becomes negligible and conduction is dominated by the T-independent excess current I_x mentioned in Eq.(16). No magnetoresistance effect was found in these diodes at any temperature.
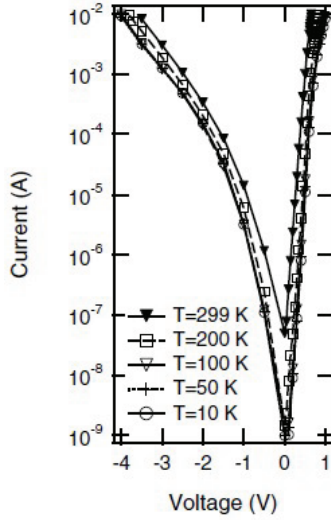
Figure 18. *Measured I-V characteristics at various temperatures in a p^+n GaMnAs/GaAs diode with a lightly doped ($N_D=10^{17}$ cm^{-3}) non-magnetic side. Reprinted with permission from H. Holmberg, N. Lebedeva, S. Novikov, P. Kuivalainen, M. Malfait, and V. V. Moshchalkov, Physica Status Solidi (a), vol. 204, pp.791-804, 2007. Copyright 2007, WILEY-VCH Verlag.*

The absence of the magnetoresistance effect in the GaMnAs/GaAs pn-junction having a lightly-doped nonmagnetic region could be due to several reasons:

i.   Since $N_D << N_A$, the lightly doped nonmagnetic side of the junction dominates the diffusion current and therefore total current does not depend on the band splitting. Also, due to the high doping of the p-side, necessary for onset of ferromagnetism, the condition for the dominance of the magnetic part of the recombination current is not fulfilled.

ii.   The conduction band splitting parameter Δ_1 can be as small as the thermal energy leading to an unsubstantial band splitting and MR effect.

iii. There is no ferromagnetic ordering in the depletion region of the diode due to the absence of free holes. Therefore the magnetic field does not change the built in potential of the diode, in contrast to the predictions of the model above, which are used as the starting point the situation depicted in Figure 15.

iv.   The excess current, which does not depend on the magnetic field, dominates at low temperatures.

4.2.3 Conclusions

We think that the absence of ferromagnetism in the depletion region of the magnetic GaMnAs/GaAs diode is the most probable reason for not observing any MR effect, not even at low temperatures. Actually, the expectations were not very high for this type p-n diode, since it is well known [49] that the dc current in the p-ndiodes is always dominated by the more lightly doped side of the diode, which in the case of Figure 15 was nonmagnetic. The situation is quite different in the case where both sides of the magnetic diode are heavily doped, as discussed in Ch.4.3 below.

4.3 Ferromagnetic Esaki-Zener Tunnelling diode

4.3.1 Modeling

When both sides of a p-n diode are so heavily doped that the corresponding Fermi levels lie within the bands (degenerated semiconductors), the overlap between the valence band on the p-side and the conduction band on the n-side enables a direct tunnelling of the electrons through the forbidden gap.[49] The tunnelling component I_{tunn} of the total current (16) changes the I-V curves drastically at the reverse bias and at small positive bias voltages, while in the high positive bias region the diffusion component I_{diff} dominates. This is shown schematically in Figure 19, where the I-V characteristics of a conventional and a tunnel diode are compared to each other.
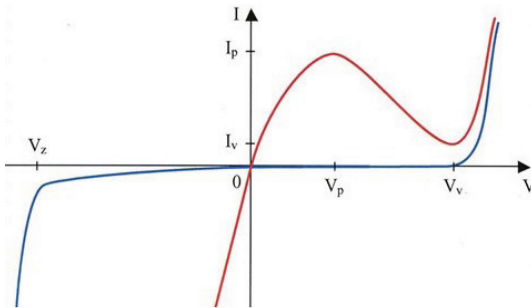

Figure 19. Schematic comparison of the I-V characteristic curves of the Esaki-Zener tunnelling (red) and conventional (blue) p-n diodes.

The dependence of the tunnelling current on the mutual orientation of the magnetization of ferromagnetic electrodes, the so-called tunnelling magnetoresistance (TMR), was first observed in metallic magnetic tunnelling junctions (MTJ) consisting of two ferromagnetic metal layers separated by a thin insulating barrier through which the carriers tunnel. [7,8] A similar effect was observed

in structures with ferromagnetic GaMnAs layers instead of metal layers. [52,53,54] Moreover, in the all-semiconductor MTJs the TMR effect is sensitive to the direction of the applied magnetic field with respect to the direction of current and crystallographic axis. This so-called tunnelling anisotropic magnetoresistance (TAMR) effect was observed in structures containing a single ferromagnetic electrode [55,56], as well as in typical MTJs with two ferromagnetic contacts [57,58].

In the case of the tunnelling diode, where the p-side is a heavily doped ferromagnetic GaMnAs layer, and the n-side is a heavily doped nonmagnetic GaAs layer, it is natural to assume that the tunnelling term I_{tunn} of the total current (16) becomes dependent on the magnetic ordering (and hence on temperature and magnetic field) due to the effect of band splitting on the density of states and due to the spin dependence of the tunnelling probability. The band diagram of the magnetic tunnel diode is shown in Figure 20.
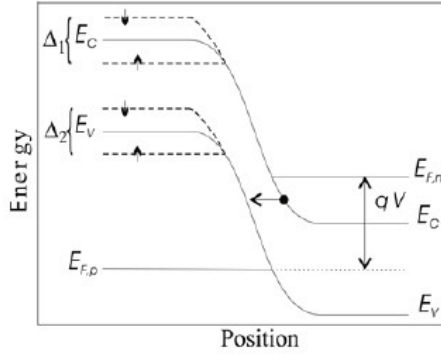
Figure 20. Schematic energy diagram for a tunnel diode, where the p-side is ferromagnetic. The dashed lines show the spin-polarized band edges. E_{Fp} and E_{Fn} are the quasi-Fermi levels for holes and electrons, and V is the applied voltage. It is assumed that there is no band splitting (ferromagnetism) in the depletion region. Reprinted with permission from H. Holmberg, N. Lebedeva, S. Novikov, P. Kuivalainen, M. Malfait, and V. V. Moshchalkov, Physica Status Solidi (a), vol. 204, pp.791-804, 2007. Copyright 2007, WILEY-VCH Verlag.

The effect of the ferromagnetic ordering and the consequent changes in the density of states (DOS) in the valence band in a GaMnAs/GaAs tunnelling diode can be estimated using the standard expression for the direct inter-band tunnelling current:

$$I_{tunn} = AC \sum_\sigma \int_{Ec(n)}^{Ev(p)} T_\sigma(E)[f_c(E) - f_v^\sigma(E)] \, D_c(E) D_v^\sigma(E) dE \qquad (19)$$

where A is the area of the diode, C is a constant that does not depend on temperature nor on the magnetic field, D_c and D_v^σ are the densities of states for conduction and valence bands, respectively, which are given by:

$$D_C(E) = \frac{M_C m^{*3/2}\sqrt{2}}{\pi^2 \hbar^3}(E - E_C)^{p_1} \tag{20}$$

$$D_V^\sigma(E) = \frac{1}{2}\frac{m_h^{*3/2}\sqrt{2}}{\pi^2 \hbar^3}\left(E_V - E - \frac{\Delta_2}{2}(\delta_{\sigma\uparrow} - \delta_{\sigma\downarrow})\right)^{p_2} \tag{21}$$

The parameters p_1 and p_2 have the value ½ in the case of parabolic bands. However, in heavily doped disordered semiconductors with tail states at energies close to the band edges these parameters can have values larger than ½. According to the calculations presented in Publication IV, the change in tunnelling probability $T_\sigma(E)$ due to the valence band splitting causes only negligible (<0,1%) changes in the tunnelling current. On the other hand, the changes in the density of states due to the band splitting can cause a sizable decrease (-5%) in the tunnelling current in the case of parabolic bands, as shown in Figure 21, where the results were calculated from Eqs.(19)-(21). This decrease in the tunnelling component of the total current through the ferromagnetic Zener-Esaki diode and its dependence on temperature and magnetic field should follow the corresponding dependences of the magnetization in the GaMnAs layer.
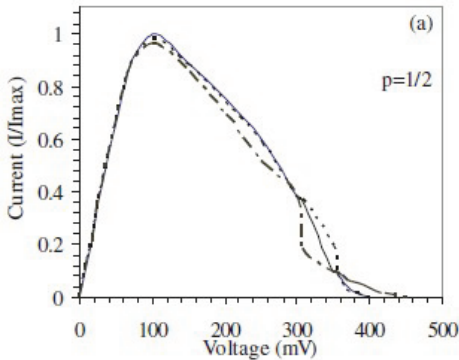

Figure 21. Calculated tunnelling current vs voltage for the tunnel diode with ferromagnetic p-side in the case of parabolic bands (p=1/2). Solid curves correspond to the case with no band splitting, the dashed and dotted curves – to Δ_2=0,1eV and Δ_2=0,2eV. Reprinted with permission from H. Holmberg, N. Lebedeva, S. Novikov, P. Kuivalainen, M. Malfait, and V. V. Moshchalkov, Physica Status Solidi (a), vol. 204, pp.791-804, 2007. Copyright 2007, WILEY-VCH Verlag.

In the calculations above the mutual orientation of the applied magnetic field and the direction of tunnelling current were not taken into account. Indeed, a more accurate model for the magnetization dependence of the tunnelling cur-

rent can be developed by taking into account not only the band splitting but also the anisotropy of the density states, i.e., its dependence on the orientation of the magnetization. The theory of anisotropic tunnelling magnetoresistance (TAMR) has been developed by several authors[59,60]. Its basic idea is the following: due to the exchange interaction there is a strong anisotropy in the Fermi surface of GaMnAs, related to the direction of magnetization, which in turn causes uniaxial anisotropic changes in the density of states (DOS) in the valence band of GaMnAs. Consequently, a rotation of the magnetization with respect to the direction of the tunnelling current by an applied magnetic field causes a change in the DOS, and according to Eq.(19), in the tunnelling current. The models [59,60] predict an in-plane TAMR effect in the GaMnAs/GaAs Esaki-Zener tunnelling diodes, the magnitude of which should be in the order of several percents at moderate magnetic fields. The spin-dependent interband tunnelling is also sensitive to the rotation of magnetization achived by applying an out-of-plane magnetic field. The magnitude of perpendicular TAMR is defined as:

$$TAMR_{\perp} = \frac{R(H_{\perp}) - R(0)}{R(0)}$$

where $R(H_{\perp})$ and $R(0)$ are the resistances in the cases of the out-of-plane and in-plane saturated magnetization, respectively. Since in the ferromagnetic GaMnAs thin films the easy axis of the magnetization lies in the plane of the film, the transverse TAMR can be observed at the temperatures lower than the Curie temperature under the application of a perpendicular-to-plane magnetic field, if it is strong enough to rotate the magnetization from the in-plane direction to the out-of-plane direction.

4.3.2 Experimental results for the spin Esaki-Zener tunnelling diode

The first experimental results for the ferromagnetic GaMnAs/GaAs tunnelling diode were published in Publication III and later in more detail in Publication IV. When during the growth of the p-n diode also the n-side was heavily doped (10^{19} cm^{-3}), we obtained the device in which the I-V curves exhibited typical features of the tunnelling diode. As shown in Figure 22, in the voltage range 0.2-0.4V there is clearly seen a negative resistance region due to the inter-band tunnelling. At low temperatures T< 100K the current becomes only weakly T-dependent, in the same way as in the conventional p-n diodes discussed above.
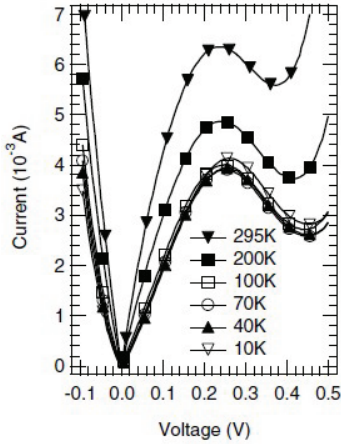
In contrast to the conventional p-n diode the *I-V* characteristics of the tunnelling diode exhibit magnetic field dependence at low temperatures mainly in the negative resistance (tunnelling) region, as shown in Figure 23. At high bias voltages, where the diffusion and excess currents dominate, no magnetoresistance was observed at any temperatures. This is in agreement with the results for the p+n diode, where the diffusion current showed no magnetic field dependence.
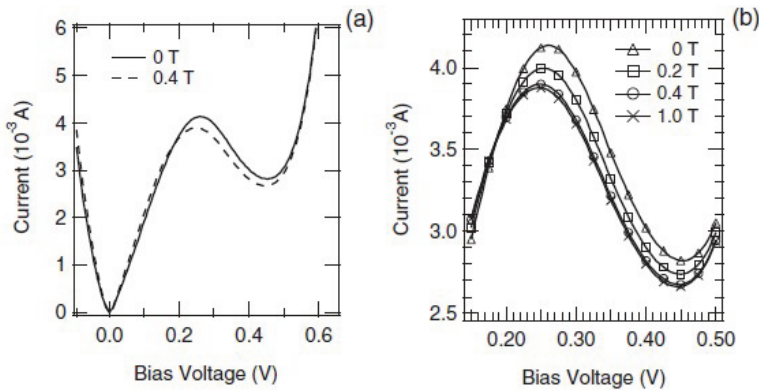
The measured peak current decrease is in good agreement with that predicted above for the tunnelling current in the case of the parabolic bands, and it has the same order of magnitude ($\Delta I/I$=8%) as the value calculated from Eq.(19) in the case of the valence band splitting parameter Δ_2=0,2eV *($\Delta I/I$=5%,* see Fig.21). As it is shown in Fig.24, the relative current change saturates in higher magnetic fields, which again is in agreement with the theory, since $\Delta I_{tunn}/I_{tunn} \sim \Delta D_v/D_v \sim \Delta_2^2 \sim \langle S^z \rangle^2$, and $\langle S^z \rangle$ saturates with increasing B.
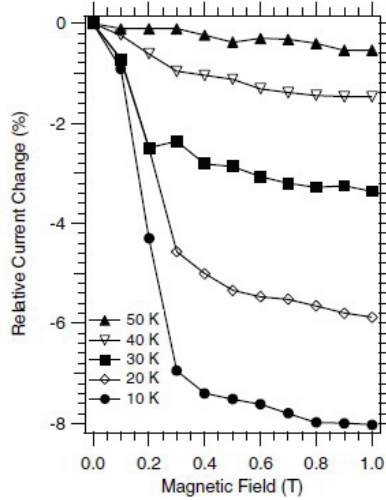

Figure 24. *Relative change of the tunnelling current (I(B)-I(0))/I(0) vs. magnetic field at various temperatures in a GaMnAs/GaAs tunnel diode near the peak voltage (V=300mV). Reprinted with permission from H. Holmberg, N. Lebedeva, S. Novikov, P. Kuivalainen, M. Malfait, and V. V. Moshchalkov, Physica Status Solidi (a), vol. 204, pp.791-804, 2007. Copyright 2007, WILEY-VCH Verlag.*

In small magnetic fields the above relation $\frac{\Delta I_{tunn}}{I_{tunn}} \sim \Delta D_v/D_v \sim \Delta_2^2 \sim \langle S^z \rangle^2 \sim B^2$ predicts a parabolic *B*-dependence for the relative current change, which is also observed in Fig.24 in the field range *B*=0-0.2T.

At low bias voltages *V*<0.2V the applied magnetic field increases the current slightly. This effect could result from a shift of the *I-V* curves towards the lower voltages due to the negative magnetoresistance of the GaMnAs layer on the ferromagnetic p-side. However, since this shift is not observed at higher voltages (V>0,5V), we have to state that its origin remains unexplained.

It is interesting to note that at the same time when we obtained the first results on the spin-dependent tunnelling published in Publication III, also another independent research group [56] published very similar results. All our ob-

served effects of the magnetic field on the conductance of ferromagnetic Zener-Esaki diode fit very well with published data on TMR in the similar device, when magnetic field is switched from in-plane to out-of-plane direction [56] , as shown in Figure 25.
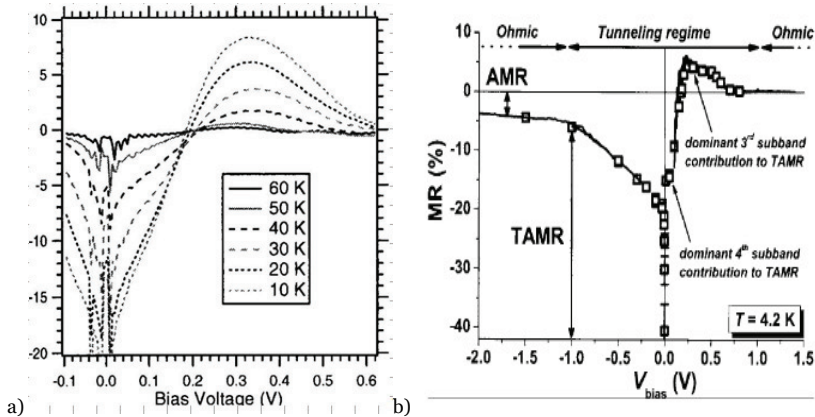
Both the negative magnetoresistance (current increases under application of magnetic field) at the low bias voltages and positive magnetoresistance for larger positive bias (tunnelling region) are seen in the results published by both groups. Therefore our results can also be related not only to the change in the DOS due to the band splitting but more accurately to the tunnelling anisotropic magnetoresistance (TAMR) effect due to the changes in the anisotropic DOS caused by the changes in the direction of the magnetization.

4.3.3 Conclusions

We have observed spin-dependent tunnelling and a large (up to 20%) magnetoresistance effect at low temperatures (10K) in the ferromagnetic GaMnAs/GaAs Zener-Esaki tunnelling diode. The MR effect is related to the spin dependence of the DOS in the ferromagnetic GaMnAs layer, or more accurately to the anisotropy in the magnetization dependence of the DOS in the

valence band. Our experimental results are in good agreement with those obtained independently by another research group. As shown in Figure 25, the large MR is seen at very low bias voltages, which could allow low power spintronic applications. Another application of the ferromagnetic tunnelling diode could be related to the electrical injection of spin-polarized carriers in a spin injector or a spin filter. The electrical spin injection from p-GaMnAs into a nonmagnetic semiconductor was first achieved by injection of spin-polarized holes (under positive bias in the tunnelling diode)[61]. Under the negative bias the spin-polarized electrons tunnel from the valence band of GaMnAs into the conduction band of the non-magnetic n-side[62]. Recently, a very high spin polarization of the injected current (80%) has been observed in such devices. [63,64]

4.4 Magnetic resonant tunnelling diode

Resonant tunnelling is a quantum phenomena that can be briefly described as follows: while the transmission probability for a particle incident on a rectangular potential barrier is always less than one, a double barrier structure can be completely transparent for particles with certain energies, namely those coincident with quantized energy levels in the quantum well (QW), formed by the potential barriers.

A resonant tunnelling diode (RTD) is a semiconductor device consisting of an emitter (heavily doped, narrow-band gap material), a quantum well between two barriers made of a large band gap material, and a collector, with electrical contacts attached to the emitter and the collector, as shown in Figure 26a. At certain values of the applied voltage the I-V characteristics of the RTD exhibit peaks that correspond to the resonant tunnelling of the charge carriers from the emitter through the quantized levels in the quantum well (HH1, LH1, HH2 for a GaAs QW) to the collector (at positive bias for the p-type device) or from collector to the emitter (at negative bias).
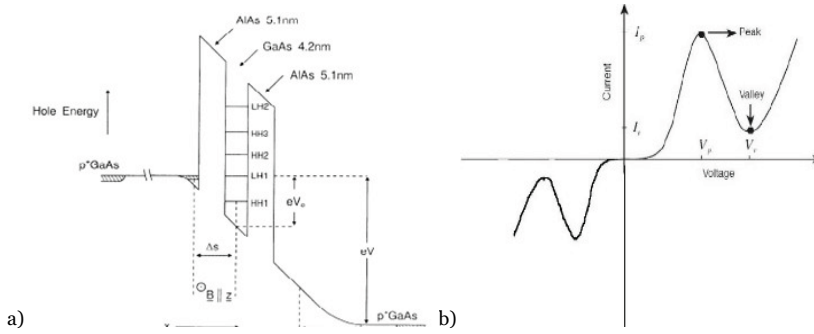
Figure 26. a) *Schematic diagram of the valence band profile of the p-type GaAs/AlAs resonant tunnelling diode under an applied voltage V.* **b)** *I-V characteristic of the RTD. Reprint with the permission from Johnny Ling, University of Rochester.*

The research of RTDs has been intensive for many decades. The effect of a magnetic field on the *I-V* characteristics of the nonmagnetic GaAs/AlAs RTD was studied for the first time by Mendez [65] and Hayden[66]. It was observed that high magnetic field ($B>2$T) applied perpendicular to the junction causes the appearance of additional maxima on the low-voltage side of the resonances due to the Landau level formation inside the quantum well (QW) [66], while the field applied parallel to the junction causes a shift of resonances due to the quantization of the charge carrier motion in the plane of the QW [65]. After the discovery of the DMS materials the study of RTDs were extended to the RTD structures having a ferromagnetic QW [69], emitter [67,68], or/and collector. In the RTD with a ferromagnetic Mn-doped GaAs emitter, fabricated by Ohno et al. [67,68], a spontaneous spin splitting of the valence band was observed in the I-V characteristics as splittings of the LH1 and HH2 resonant peaks, which appeared at $T<T_c$ and increased with the magnetic field in good agreement with the theory presented below.

4.4.1 Modeling of the RTD with a ferromagnetic emitter.

Modeling of non-magnetic RTDs is a mature field, but recently also magnetic RTDs with a ferromagnetic emitter or a QW have been modeled by several groups.[70-73] The magnetic RTD with the ferromagnetic emitter is obtained from the non-magnetic RTD shown in Figure 26a simply by doping heavily the uppermost GaAs layer with Mn. In the case of a symmetrical quantum well and under a positive bias the device acts as a RTD with a ferromagnetic emitter, and under a negative bias it acts as a RTD with a ferromagnetic collector, as

shown in Figure 27. At temperatures below T_c spontaneous band splitting in the magnetic layer is expected to change the *I-V* characteristics of the device. These changes are expected to be more prominent for a hole injection from the ferromagnetic emitter into the non-magnetic collector (positive bias), than for a hole injection from the non-magnetic emitter into the ferromagnetic collector (negative bias).
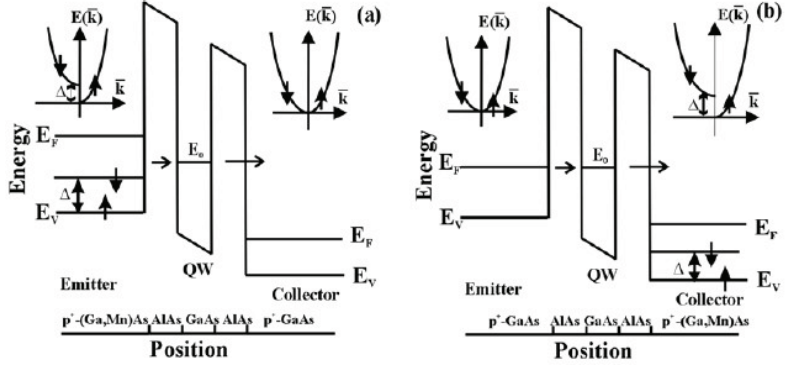

***Figure 27**. Band diagram for RTD with **a)** a ferromagnetic emitter, and **b)** with a ferromagnetic collector, in both cases the band splitting is non-zero, Δ>0. Reprinted with permission from H. Holmberg, N. Lebedeva, S. Novikov, P. Kui- valainen, G. Du, X. Han, M. Malfait, and V. V. Moshchalkov, Physica Status Sol- idi (a), vol. 204, pp.3463-3477, 2007. Copyright 2007, WILEY-VCH Verlag.*

A straightforward way to model a RTD with a ferromagnetic emitter is to modify the well-known Tsu-Esaki formula[74] for the tunnelling current by tak- ing into account the band splitting Δ. Then the total current including the spin- up and spin-down contributions is given by

$$I_{tot} = I_{tot}^{\uparrow} + I_{tot}^{\downarrow} = \int_0^{\infty} T_{\uparrow}(E)S_{\uparrow}(E)dE + \int_{\Delta}^{\infty} T_{\downarrow}(E)S_{\downarrow}(E)dE \qquad (22)$$

where $T_{\sigma}(E)$ is the quantum mechanical transmission coefficient through the double barrier structure given by the following Lorenzian:

$$T_{\sigma}(E) = \frac{\Gamma_L \Gamma_R}{\left(\frac{\Gamma}{2}\right)^2 + (E - E_0^{res})^2} \qquad (23)$$

Here $\Gamma = \Gamma_L + \Gamma_R$ is the spin-independent full width of the half-maximum of the resonance. The partial widths Γ_L and Γ_R for the left and right barriers, re- spectively, can be calculated in a straightforward manner in the case of rectan- gular barriers.[75] In Eq.(22) the bottom of the spin-up subband was taken as a zero energy level and the energy of the resonant level can be written as:

$$E_\sigma^{res} = E_0 - \frac{qV_{QW}}{2} + \frac{\Delta}{2}\left(\delta_{\sigma\uparrow} - \delta_{\sigma\downarrow}\right) \qquad (24)$$

where E_0 is the energy of the single quantized level in the QW in the absence of band splitting and the voltage over the double barrier structure V_{QW} is assumed to be divided equally between the two barriers. The spin-dependent supply function $S_\sigma(E)$ in Eq.(22) is given by:

$$S_\sigma(E) = \left(\frac{qm^*kT}{4\pi^2\hbar^3}\right)\ln\left[\frac{1+e^{(E_{F\sigma}^L - E)/kT}}{1+e^{(E_{F\sigma}^R - E)/kT}}\right] \qquad (25)$$

The effect of the band splitting on the total current as calculated from Eq.(22) is shown in Figure 28. Here we have added a magnetization-independent leakage current to the total current (Publication VI).
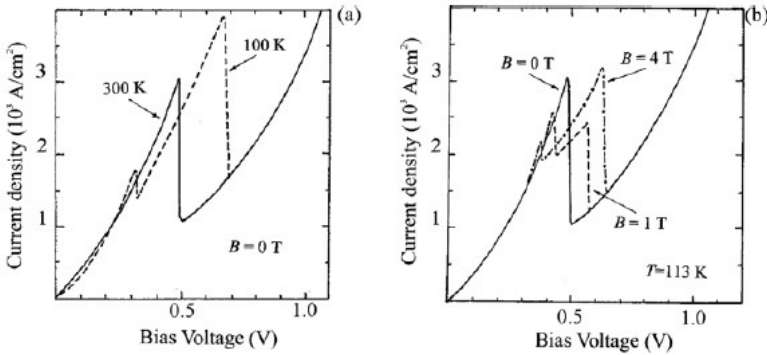

Figure 28. a) *Calculated I-V characteristics of FRTD with ferromagnetic emitter (T_c=110K), without external magnetic field **b)** Calculated effect of the external magnetic field on the I-V characteristics of FRTD with ferromagnetic emitter at temperature near T_c (113K, T_c=110K). Reprinted with permission from H. Holmberg, N. Lebedeva, S. Novikov, P. Kuivalainen, G. Du, X. Han, M. Malfait, and V. V. Moshchalkov, Physica Status Solidi (a), vol. 204, pp.3463-3477, 2007. Copyright 2007, WILEY-VCH Verlag.*

The spontaneous band splitting in the ferromagnetic emitter leads to the splitting of the resonant peak, and the peaks drift apart with increasing magnetic field. Both these effects have been observed experimentally by Ohno *et al.*[67,68]

Also in the case of a ferromagnetic collector the band splitting can have an effect on the tunnelling current due to the small change in the density of states (DOS) in the valence band. The situation is similar to that of the Zener diode, discussed above, since in the RTD structure the tunnelling current also depends on the DOS of the collecting side.

In Publication VII we have analyzed theoretically also the case where the quantum well is ferromagnetic whereas the rest of the RTD structure is non-magnetic. The transmission through the ferromagnetic QW was calculated using Green's function technique. The results predict that the effect of the splitting of the quantized energy levels inside the QW should lead to even more pronounced changes in the *I-V* characteristics than in the case, where only the emitter is ferromagnetic. However, we did not succeed in fabricating the ferromagnetic quantum wells, since the ferromagnetism disappears in very thin GaMnAs layers. Therefore, the predictions of our model in Publication VII were verified by comparing them to the experimental results obtained by other groups on magnetic ErAs/AlAs [76] and ZnMnSe/BeSe RTDs. [77]

4.4.2 Experimental

RTD structures with ferromagnetic emitters (FRTD) were grown using both the molecular beam epitaxy (MBE) and metal-organic chemical vapor deposition (MOCVD) growth techniques. First, the quantum well structure consisting of the undoped GaAs layer between two undoped AlAs barriers (all layers 5 nm thick) was grown by MOCVD on top of the p+ GaAs layer. Then a 500 nm thick Mn-doped ferromagnetic GaAs layer was grown on top of the structure using the low-temperature MBE. The front contact to the device was made by lift off process for an e-beam evaporated Au/Ti/Au metal layer. Then the wafer was patterned into separate devices by etching the 100µm wide mesa structures to the depth of 600 nm. Back contact was made by evaporating the same combination of metals as for the front contact. Thickness of the contact metals was increased by electroplating 50µm of copper. Finally the RTDs were mounted on sample holders and Al wires (100µm diam.) were bonded to the contact pads. The schematic structure of the fabricated RTD is shown in Figure 29. As a reference a nonmagnetic RTD without the Mn doping in the top layer, having otherwise the same parameters as the magnetic RTD, was fabricated. In addition, in order to characterize the magnetotransport properties of the Mn doped emitter layer, separate GaMnAs films having the same Mn concentration as the emitters of magnetic RTDs were fabricated. Resistivity, magnetoresistance and Hall effect were measured as a function of temperature for these GaMnAs films in order to prove the ferromagnetism of the RTD emitters and to determine their magnetotransport properties.
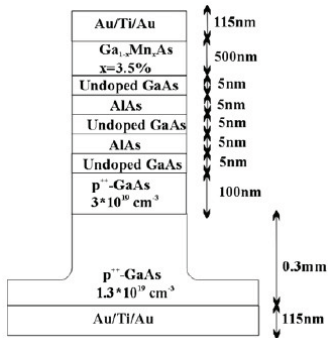
Figure 29: Schematic structure of the fabricated magnetic RTD. The structure of the non-magnetic reference device was the same excluding the Mn-doping in the uppermost layer, where Mn was replaced by beryllium. Reprinted with permission from H. Holmberg, N. Lebedeva, S. Novikov, P. Kuivalainen, G. Du, X. Han, M. Malfait, and V. V. Moshchalkov, Physica Status Solidi (a), vol. 204, pp.3463-3477, 2007. Copyright 2007, WILEY-VCH Verlag.

The *I-V* characteristics of two ferromagnetic RTDs, one with a metallic emitter and one with a semiconducting emitter, and a non-magnetic reference RTD were measured in the temperature range 8-300K without the magnetic field and in the magnetic field (0-1T) applied perpendicular to the plane of the device.

4.4.3 Experimental results

Fig. 30 shows the measured *I-V* characteristics of the nonmagnetic RTD. The first three resonant peaks corresponding to the quantized HH1, LH1 and HH2 energy levels in the AlAs/GaAs/AlAs QW are clearly seen in both bias polarities (see also Figure 26). The inset shows that in the nonmagnetic RTD the magnetic field dependence of the tunnelling current is minor (<0.3%). Therefore, the observed larger changes in the I-V characteristics below must be related to the Mn doping.
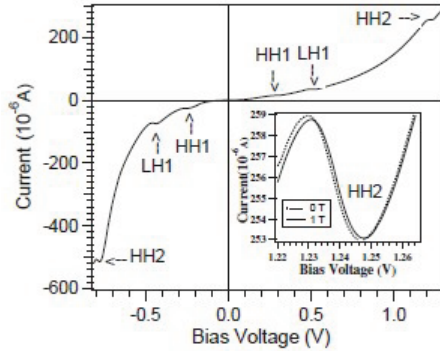
Figure 30: *I-V characteristics of a non-magnetic AlAs/GaAs RTD at 8K. The inset shows effect of magnetic field on the HH2 resonant peak. Reprinted with permission from H Holmberg, G Du, N Lebedeva, S Novikov, M Mattila, P Kuivalainen1 and X Han Journal of Physics: Conference Series 100 (2008) 052074*

In the case of the RTD with a ferromagnetic (metallic) emitter we could not observe any resonant peak at the positive bias, i.e., in the case of the hole injection from the ferromagnetic emitter into the quantum well. However, at the negative bias all the peaks were present, as shown in Figure 31. This is probably due to the fact that the Fermi energy in the heavily Mn-doped emitter (200 meV for p=10^{20} cm^{-3}) is comparable with the spacing between the first resonances and the details of the quantized levels in the QW are just smeared out in the I-V characteristics at the positive bias.
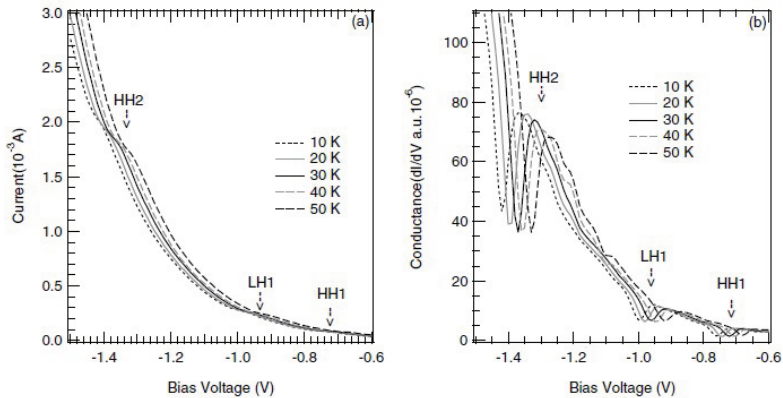

Figure 31. a) *I-V characteristics of the FRTD with a metallic GaMnAs emitter at various temperatures.* *b)* *Conductance dI/dV vs. bias voltage at different temperatures for the same device. Reprinted with permission from H. Holmberg, N. Lebedeva, S. Novikov, P. Kuivalainen, G. Du, X. Han, M. Malfait, and V. V. Moshchalkov, Physica Status Solidi (a), vol. 204, pp.3463-3477, 2007. Copyright 2007, WILEY-VCH Verlag.*

In the case of the FRTD with the semiconducting emitter, where Fermi energy in the emitter is smaller than that in FRTD with metallic emitter, also the first HH1 resonant peak was observed at the positive bias, as shown in Figure 32.
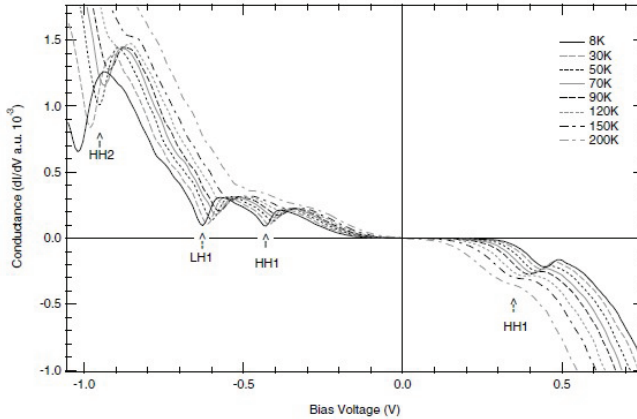
At the negative bias voltages, i.e., in the case where the holes are injected from the nonmagnetic collector through the quantum well into the magnetic emitter, the dependence of the *I-V* characteristics on the magnetic field is expected to be weak.[70] Figure 33 shows the magnetic field dependence of the *I-V* characteristics of the FRTD with the metallic emitter measured around the resonant peak HH2, where this dependence is most pronounced.
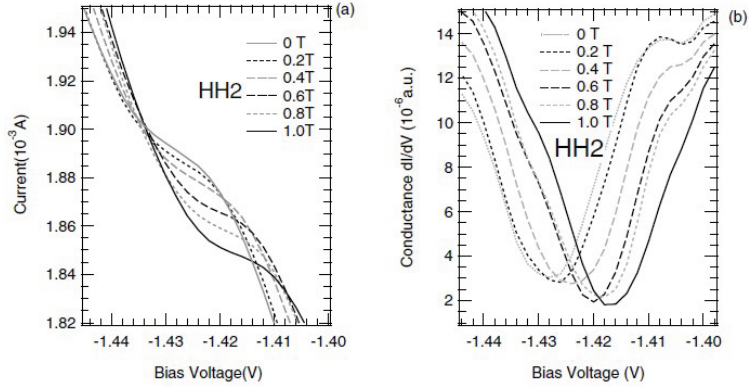
Figure 33. a) *I−V characteristics of the magnetic RTD with a metallic emitter in various magnetic fields at T = 8 K for negative bias voltages around the resonance peak HH2.* *b)* *Conductance dI/dV vs. negative bias voltage in various magnetic fields at T=8K. Reprinted with permission from H. Holmberg, N. Lebedeva, S. Novikov, P. Kuivalainen, G. Du, X. Han, M. Malfait, and V. V. Moshchalkov, Physica Status Solidi (a), vol. 204, pp.3463-3477, 2007. Copyright 2007, WILEY-VCH Verlag.*

Two effects can be observed as the magnetic field increases: a shift of the *I-V* characteristics towards lower voltages and a decrease in the current. The first effect can be due to the negative magnetoresistance of the emitter, whereas the second one can be explained by a magnetic field dependence of DOS in the ferromagnetic collector, as discussed above. However, the simple model, Eq. (22), predicts that the MR effect should be largest at temperatures close to T_c, where the magnetic field dependence of the band splitting parameter is largest, whereas we observed that MR was largest at low temperatures well below T_c. As in the case of the Esaki-Zener tunnel diode, this observation is more consistent with the tunnelling anisotropic magnetoresistance (TAMR) model, in which a change in the direction of the saturated magnetization causes the MR effect at low temperatures. Originally, in the case of zero field, magnetization lies along the easy axis in the plane of the GaMnAs film, and a magnetic field applied perpendicularly to the plane of the device re-orients it, which in turn causes a change in the tunnelling current due to the dependence of the anisotropic DOS on the direction of magnetization. [59,60]

An interesting effect observed in the FRTD with a semiconducting emitter was the appearance of a resonant peak splitting at low temperatures, as shown in Figure 34. This effect is similar to the one reported by Ohno et al. [67,68] In our case, however, this could hardly be interpreted as a manifestation of a spontaneous valence band splitting, since (i) double peak structures appear also in non-magnetic RTDs, (ii) they appear at negative bias that corresponds to hole

injection from the non-magnetic collector, (iii) they appear at different temperatures for different peaks, and (iv) the observed voltage difference between the peaks does not depend on temperature nor the magnetic field, as shown in Figure 34.
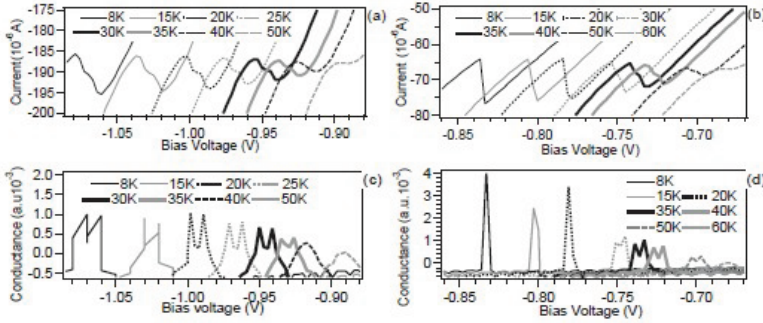

Figure 34. a) and **b)** show the I-V characteristics of a FRTD with a semiconducting (Ga,Mn)As emitter at various temperatures for the first two peaks HH1 and LH1. **c)** and **d)** show the conductance dI/dV vs. the negative bias voltage at various temperatures for the first two peaks (B= 0T in all cases). Reprinted with permission from H Holmberg, G Du, N Lebedeva, S Novikov, M Mattila, P Kuivalainen1 and X Han Journal of Physics: Conference Series 100 (2008) 052074

Figure 35. (a) Effect of an external magnetic field on the I-V characteristics of a FRTD with a semiconducting emitter at T = 8 K for negative bias voltages. **(b)** Effect of an external magnetic field on conductance dI/dV vs. the negative bias voltage at T=8K. Reprinted with permission from H Holmberg, G Du, N Lebedeva, S Novikov, M Mattila, P Kuivalainen1 and X Han, Journal of Physics: Conference Series 100 (2008) 052074
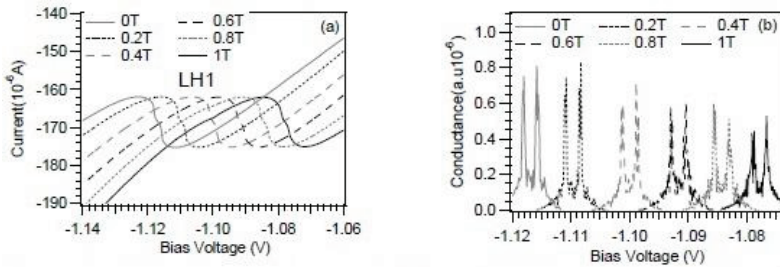
These phenomena could be attributed to the appearance of Landau levels in the QW under application of a magnetic field. However, for some peaks the splitting disappears at low temperatures (Fig.34d), which eliminates this interpretation. We believe that a more probable explanation for the observed double-peak structure is related to the instability of the measurement circuit due to the negative differential resistance of the ferromagnetic RTD[78].

4.4.4 Conclusions

Our theoretical models for the ferromagnetic resonant tunnelling diodes predict large changes in the I-V characteristics as a function of temperature and magnetic field at temperatures close to the ferromagnetic transition temperature. Indeed, the effect of the band splitting due to the spontaneous magnetization has been observed experimentally in RTDs having a ferromagnetic emitter.[67,68] In our RTDs with ferromagnetic GaMnAs emitters the resonant peaks in the measured I-V characteristics, related to the quantized energy levels inside the quantum well, could be observed clearly. However, in our experiments the heavy doping with Mn and the consequent large Fermi energy prevented us from observing the band splitting directly. A small magnetoresistance effect was observed in some peaks, which was interpreted to be a consequence of the T- and B-dependent changes in the density of states in the valence band due to the band splitting. This interpretation is in accordance with the similar conclusion made above in the case of the ferromagnetic Esaki-Zener diodes.

4.5 Ferromagnetic quantum dots

4.5.1 Electronic structure and fabrication of quantum dots

A semiconductor quantum dot (QD) is a nanostructure, or an artificial molecule, which shows a quantum confinement of the charge carrier energies in three dimensions due to its small size: typical QD dimensions are of the order of 10 nm or less.[75] A crude approximation for the electronic states of a QD can be obtained by solving the Schrödinger equation for a particle in a box: [75]

$$E_{lnm} = \frac{l^2 \hbar^2 \pi^2}{2m^* L_x^2} + \frac{n^2 \hbar^2 \pi^2}{2m^* L_y^2} + \frac{m^2 \hbar^2 \pi^2}{2m^* L_z^2} \qquad (26)$$

Here l, n, and m are integers, and L_x, L_y, and L_z are the dimensions of the QD in the x-, y-, and z-directions, respectively. The spectrum of energies and thus the density of states are completely discrete with degeneracies due to spin and multiple valleys in the energy bands of the semiconductor of which the dot is made. In a more realistic quantum dot model the shape of the dot is assumed to be disk-like with a radius R_0 and a height z_0, the confining potential is assumed to be harmonic in the lateral direction and quantum well-type in the z-direction (Publication VIII).

Typically the transport through the dot can be studied experimentally by contacting the dot with metal contacts, as shown schematically in Figure 36a. An additional electrode beside the dot may act as a gate resulting in a single elec-

tron transistor.[79] Figure 36b shows the simplified electronic structure of a QD, when only the most relevant electronic states are considered. If the dot energy level ε_d is occupied by an electron with spin-up, the other electron entering the dot must be at the level ε_d+U with spin-down, in accordance with Hubbard's approximation.[80] Here U is the repulsion energy between two electrons on the dot. Its value depends on the size of the dot (decreases as the dot grows larger), and it can be estimated using the first order perturbation theory for the Coulomb interaction $W_{ee}=e^2/4\varepsilon\pi r$, leading to $U=\langle 00|W_{ee}|00\rangle\approx 30meV$ for $R_0=z_0=10nm$ (Publication VIII).

The Coulomb interaction between the dot electrons results in a so-called Coulomb blockade effect [75] , in which the electron entering the dot must surmount the repulsive energy caused by the electron already occupying a dot state. The Coulomb blockade effect leads to the existence of two conductance channels through the dot: one of them corresponds to adding of an electron when the upper level is empty and another to adding an electron with the opposite spin, when the lowest level is already occupied. Experimentally, one can move between the conductance peaks by adjusting ε_d, which in practice is done through the gate voltage.
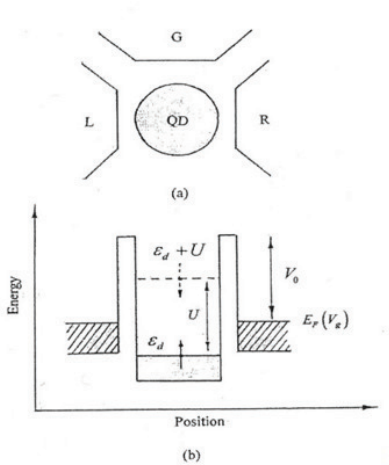

Figure 36. *(**a**) Schematic drawing of a quantum dot (QD) interacting with the left (L) and right (R) contacts via tunnelling through the potential barriers. (**b**) Electronic structure of a quantum dot showing the discrete energy levels on the dot and the metallic-like contacts having Fermi energy E_F, which can be changed with respect to the dot level by the gate (G) voltage V_g. U is the Coulomb repulsion between two electrons in the dot.*

Conductance oscillations due to the Coulomb blockade effect have recently been observed in a single InAs semiconductor dot on GaAs substrate, as shown

in Figure 37. The most difficult part of the fabrication was to make the electrical contacts to the dot. This was carried out using an electron-beam technique.[81]
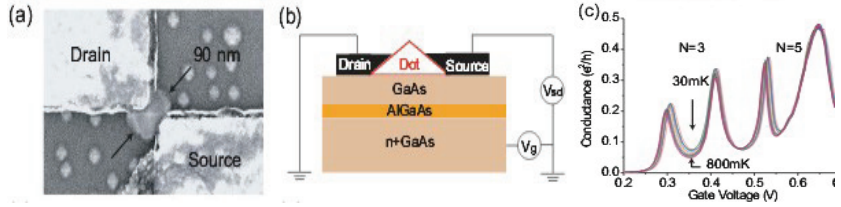

Figure 37. (a) Scanning electron microscope image of the nanogap electrodes placed on a self-assembled InAs dot. *(b)* A schematic cross-sectional view of the device. *(c)* Conductance oscillations with gate voltage under small source-drain bias measured at low temperatures (30-800 mK). Reprinted with permission from Y. Igarashi, M. Jung, M. Yamamoto, A. Oiwa, T. Machida, K. Hirakawa, and S. Tarucha Physical Review B, vol. 76, 081303 (R) (2007). Copyright 2007, The American Physical Society.*

Interesting novel possibilities arise when QD structures are combined with magnetic semiconductors. Such magnetic QDs have been grown using II-VI semiconductors CdMnTe/ZnTe [82,83] or CdSe/ZnMnSe.[84] In this way magnetic quantum dots with a few or even a single Mn atom(s) in the dot can be fabricated[85,86] . An advantage of the magnetic QDs is that they offer a way to study the interaction between a controlled number of electrons and the magnetic ions. A versatile control of the number of carries, spin, and the quantum confinement could lead to improved transport, optical and magnetic properties.[87]

Recently the first high T_C ferromagnetic semiconductor quantum dots have been grown using Co-doped CdSe [88] and ZnO [89], and Mn-doped InAs[90]. Also the first single electron transistor made of ferromagnetic Mn-doped GaAs has been reported, which, in addition to Coulomb blockade oscillations, showed a large anisotropic magnetoresistance effect at low temperatures.[91]

We have also grown self-organized magnetic InMnAs quantum dots on GaAs substrate using MBE, as shown in Figure 38. A small (a few percent) lattice mismatch between the substrate and the grown material produces a stress in the grown film, which breaks up into tiny pyramid-shaped islands. With more layers grown the pyramids self-organize and coarsen, becoming dome-shaped islands. Some of our grown samples exhibited ferromagnetism even at room temperature, as shown in Figure 39.
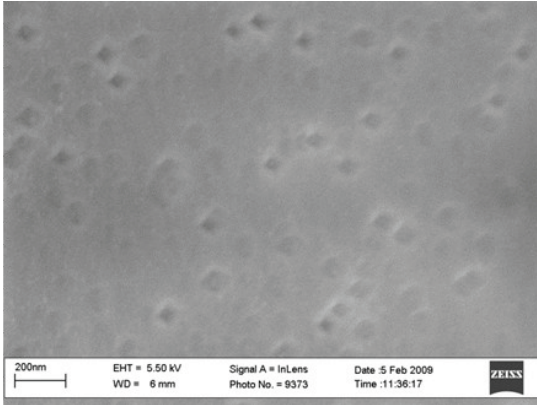
Figure 38. SEM image of the MBE grown self-organized InMnAs quantum dots on a GaAs substrate.
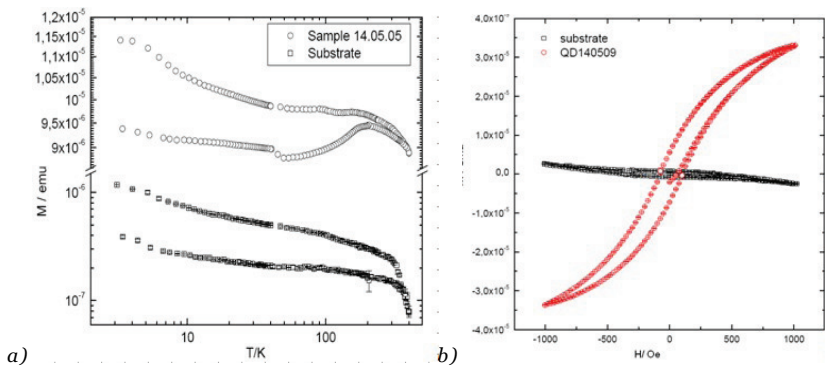

Figure 39 a) Magnetization vs. temperature in a InMnAs quantum dots on GaAs substrate (Fig. 38) as measured by SQUID magnetometer exhibiting high temperature ferromagnetism. b) Hysteresis measured at 4 K. Signal from pure GaAs substrate was measured separately and presented for comparison

4.5.2 Modeling of the ferromagnetic quantum dots and single-electron transistors

In the case of the quantum dots made of the ferromagnetic semiconductor (FSQD) different effects related to ferromagnetic ordering and large spin fluctuations should be taken into account, such as a dot level splitting due to the sp-d exchange interaction and a level broadening due to the spin disorder scattering. Figure 40 shows the electronic structure of a FSQD in the presence of the splitting of the energy levels.
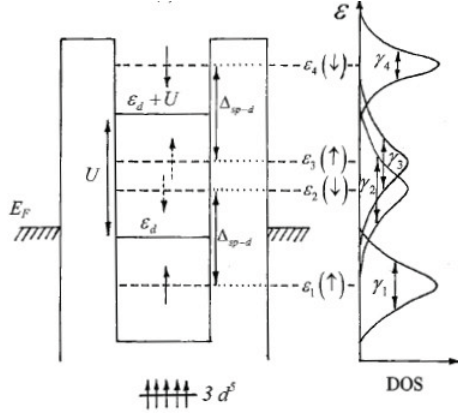
Figure 40. *Energy diagram of a ferromagnetic semiconductor quantum dot (FSQD) including two-spin degenerate dot levels ε_d and ε_d+U with the on-site Coulomb repulsion U. The two levels are split into four levels due to the giant Zeeman splitting caused by sp-d exchange interaction between the charge carriers and magnetic 3d electrons of the magnetic Mn ions on the dot. The exchange interaction also broadens the levels, as shown schematically in the density of states (DOS). Reprinted with permission from N. Lebedeva, H. Holmberg, and P. Kuivalainen, Physical Review B, vol. 77, p.345308, 2008. Copyright 2008, The American Physical Society.*

In Publication VIII spin-dependent quantum transport through the FSQD has been studied theoretically by calculating the temperature and magnetic field dependencies of the conductance in the Coulomb blockade regime. The detailed model for a FSQD included a large on-site Coulomb repulsion and the strong *sp-d* exchange interaction between the charge carriers and magnetic ions. Also terms describing charge carriers in nonmagnetic leads and tunnelling processes were included in the total Hamiltonian of the system. The spectral densities, which are needed in the calculation of the conductance, level occupations and spin accumulation, were obtained from the retarded Green functions for the FSQD. It was calculated by means of Zubarev's double-time-Green's function technique[92], also called an equation of motion (EOM) method[93]. After the Green's function $G(\varepsilon, T, B)$ had been determined, the linear magnetoconductance $g = \lim_{V \to 0} \partial I/\partial V$ could be calculated in the wide-band limit using a Landauer-type formula generalized to interacting systems[94,95]:

$$g(T, B) = \frac{e^2}{\hbar^2} \frac{\Gamma_L \Gamma_R}{\Gamma_L + \Gamma_R} \sum_\sigma \int_{-\infty}^{\infty} d\varepsilon \frac{1}{\pi} \text{Im} G(\varepsilon, T, B) \frac{\partial n_F}{\partial \varepsilon} \tag{27}$$

where $\Gamma_L \Gamma_R$ is the coupling constant between the dot and the left (right) electrode, and n_F is the Fermi-function.

Figure 41 shows the calculated conductance through the FSQD vs. Fermi energy (or gate voltage) at $T \ll T_c$ and B=0T for various values of the Coulomb

repulsion parameter U. Other material parameters are those of Mn-doped GaAs (Publication VIII). For small values of U (5 meV or less) there is only one peak since even at low temperatures the level broadening washes out the sharp resonances. For larger values of U two peaks appear in the conductance, split by $U+\Delta^d_{sp-d}$, the left one corresponding to transport of the spin-up carriers and the right one to transport of the spin-down carriers. According to Figure 40 in the presence of the band splitting there are four different energy levels, and, therefore, one would expect that there also would appear four peaks in the conductance curve in Figure 41. However, the suppression of the other two peaks follows from the dependence of the spectral density of each level on the occupancy of the other level, as reported previously by Meir *et al.* [94]
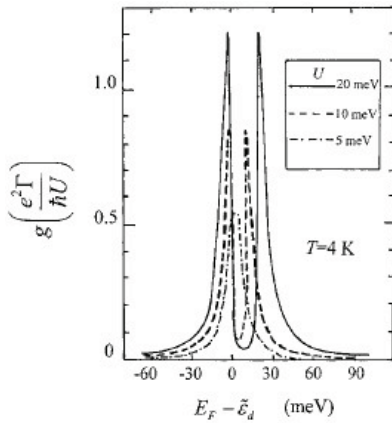

Figure 41. *Conductance through the FSQD vs. energy difference between the Fermi level E_F and the dot level ε_d (or vs. the gate voltage) at $T<<Tc$ and $B=0T$ for various values of the Coulomb repulsion parameter U. Reprinted with permission from N. Lebedeva, H. Holmberg, and P. Kuivalainen, Physical Review B, vol. 77, p.345308, 2008. Copyright 2008, The American Physical Society.*

When T approaches T_c the conductance peaks become less distinct since the level broadening has its maximum at the Curie temperature, as shown in Figure 42. At $T>T_c$ the peaks become more clear again until the thermal effects smear them out at high temperatures $T>>T_c$.
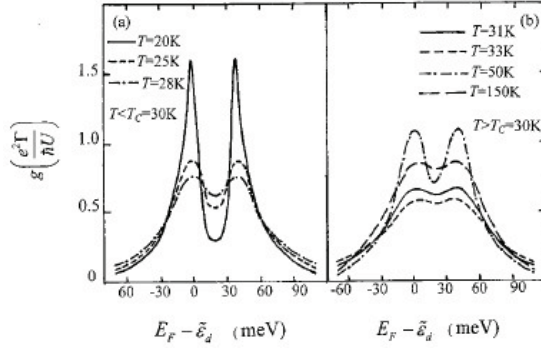
Figure 42. *Conductance through the FSQD vs. energy difference between the Fermi level E_F and the dot level ε_d (or vs. the gate voltage) at various temperatures. (a) below T_c, and (b) above T_c, when $B=0T$. Reprinted with permission from N. Lebedeva, H. Holmberg, and P. Kuivalainen, Physical Review B, vol. 77, p.345308, 2008. Copyright 2008, The American Physical Society.*

The effect of the external magnetic field on the conductance is shown in Figure 43. The conductance peaks become narrower under the application of magnetic field since the field reduces the broadening of the dot levels.
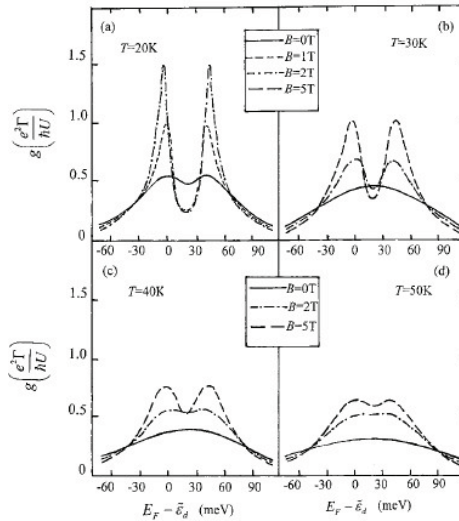
Figure 43. *Conductance through the FSQD vs. energy difference between the Fermi level E_F and the dot level ε_d (or vs. the gate voltage) at various temperatures and at various magnetic fields, when $T_c=50K$. Reprinted with permission from N. Lebedeva, H. Holmberg, and P. Kuivalainen, Physical Review B, vol. 77, p.345308, 2008. Copyright 2008, The American Physical Society.*

We also noticed a decrease of the minimum conductance between the conductance peaks with increasing temperature at $T > T_C$ (Publication VIII). This result together with those depicted in Figures 42 and 43 are exactly the ones

observed in the so-called Kondo resonance in the conductance of the nonmagnetic single electron transistors.[96-99] According to the theory, the Kondo resonance is a complicated many-particle phenomena, which results from the higher order correlations in the metallic leads of the transistor. In our theory, we completely neglected these correlations, so that the behavior shown in Figures 42 and 43 has nothing to do with the many-particle effects, but instead it is a consequence of the temperature and magnetic field dependences of level broadening in FSQDs. It also is interesting to notice that our model predicts that in FSQDs the Kondo-like behavior should appear at much higher temperatures than the ordinary Kondo effect in the nonmagnetic SETs.

4.5.3 Conclusions

Due to the strong exchange interaction between the charge carriers and the magnetic ions the electrical transport properties of the ferromagnetic single electron transistors (FSETs) depend more strongly on temperature and magnetic field than the same properties in the nonmagnetic devices. An interesting finding was that our theoretical model predicts all the typical features of the Kondo resonance for the conductance in the case of the FSET. We have fabricated ferromagnetic InMnAs quantum dots on GaAs substrate and determined their magnetic properties, but in the next phase we still have to develop a fabrication technique for the metal contacts to the QD.

5 Summary

Spin electronics based on magnetic semiconductors could offer many advantages over the present commercial spintronic devices, which are made of ferromagnetic metal thin films. These advantages include, e.g., an easier integration with conventional microelectronics, a better sensitivity to magnetic fields, and a possibility to fabricate multifunctional devices showing, e.g., current amplification and rectification. In the present work Mn-doped GaAs was chosen as the semiconductor material, because the GaAs device technology is a mature field, the physical properties of GaAs are well known, and the reproducible doping of GaAs with Mn atoms can be controlled accurately.

In the theoretical part of the work various models for the magnetotransport properties of the GaMnAs thin films and the basic ferromagnetic device structures were developed. In some cases semiclassical modeling techniques were used, but in most cases the advanced Green's function techniques were utilized. They turned out to be very versatile allowing an accurate modeling not only in the cases of the various magnetic diodes but also in the cases of the smallest nanodevices such as ferromagnetic single electron transistors made of magnetic semiconductor quantum dots. Most of the model predictions could be verified by comparing them to experimental results obtained in the present work or by other research groups. Some totally unexpected novel results were obtained such as the prediction of a Kondo-like conductance resonance at high temperatures in ferromagnetic single electron transistors.

In the experimental part of the work various spintronic semiconductor devices were fabricated and characterized, such as ferromagnetic pn-diodes, Esaki-Zener diodes, and resonant tunnelling diodes. The magnetic diode structures were fabricated using low-temperature molecular beam epitaxy and metal-organic chemical vapor phase epitaxy techniques. It was shown that by adding a few percent of Mn in GaAs many transport properties become magnetic field dependent. Especially, it was found that the ferromagnetic Esaki-Zener tunnel diodes show large magnetoresistance and spin-dependent tunnelling effects, which are related to the strong exchange interaction between the charge carriers and the magnetic atoms in the Mn-doped GaAs layer. Ferromagnetism in the grown GaMnAs layers was confirmed by resistivity, Hall-effect and direct magnetization measurements.

One of the most important findings was the observation of the large tunnelling anisotropic magnetoresistance at very low bias voltages in the Esaki-Zener diodes, which could pave the way to low-power spintronics. Also the magnetic quantum dots and single electron transistors might act as miniaturized memory elements, where the magnetic properties could be controlled by the gate voltage. However, although the Mn-doped GaAs is an optimal material for testing various ideas and proposals for novel spintronic devices, the real applications of the spintronic semiconductor devices would require materials having much higher Curie temperatures as well as showing ferromagnetism also in more lightly doped regions of the device structure. In this respect a promising finding in the present study was the observation of high temperature ferromagnetism in the Mn-doped InAs quantum dots.

6 References

[1] A.Fert, J.George, H.Jaffres, R.Mattana and P.Seneor, Electrophysics News **34** (6) (2003)

[2] M.Johnson, R. H. Silsbee, Phys. Rev. Lett. **55** (17), pp.1790–1793(1985).

[3] M.N. Baibich, J.M. Broto, A.Fert, F.Nguen Van Dau, F.Petroff, Phys. Rev. Lett. **61**, pp.2472-2475 (1988)

[4] G. Binasch, P.Grunberg, F.Saurenbach and W.Zinn, Phys.Rev B **39**, pp.4828-4830 (1989)

[5] N.F.Mott, Proc. Roy.Soc. A 153, p.699 (1936)

[6] P.M.Tedrow and R.Meservey, Phys. Rev. B **8**, pp.5098-5108 (1973)

[7] M.Julliere, Physics Letters A **54** (3), pp. 225–201 (1975).

[8]F.Matsukura, H. Ohno, A.Shen and Y.Sugawara, Phys. Rev B **57**, pp.R2037-R2040 (1998)

[9] A.Mauger and C.Godart, Phys. Rep. **141**, p.51 (1986)

[10]H.Ohno, F.Matsukura and Y.Ohno, Solid State Communications **119**, pp.281-289 (2001)

[11] I.Arata, Y.Ohno, F.Matsukura and H.Ohno, Physica E (Amsterdam) **10**, pp.288-291 (2001)

[12] M.Jain, L.Kronic, J.R. Chelikovski and V.V. Godlevsky, Phys. Rev. B **64**, pp.245205,1-5(2001)

[13]"Diluted Magnetic Semiconductors", edited by M.Balkansky and M.Averous (Plenum, New- York, 1991)

[14]J.K. Furduna and J.Kossut, "Semiconductors and Semi-metals" (Academic, New-York,1988),Vol. 25

[15]T.Dietl, "Handbook of Semiconductors" (North Holland, Amsterdam, 1994) Vol. 38

[16] H.Ohno, A. Shen, F.Matsukura, A.Oiwa, H.Endo, S.Katsumoto and Y.Iys, Appl. Phys. Lett. **69**(3) pp.363-365 (1996)

[17]H.Ohno, H.Munekata, T.Penney, S. Von Molnar and L.L.Chang, Phys. Rev. Lett. **68**, pp.2664-2667 (1992)

[18] H.Munekata, H.Ohno, S. Von Molnar, A. Segmuller, L.Chang and L.Esaki, Phys. Rev. Lett. **63**, pp.1849-1852 (1989)

[19] I.Zutic, J.Fabian and D.Sarma, Review of Modern Physics **76**, p.323 (2004)

[20] K. Olejnik , M. H. S. Owen, V. Novák, J. Mašek, A. C. Irvine, J. Wunderlich, and T. Jungwirth, Phys. Rev. B **78** pp. 054403, 1-4 (2008).

M.Wang , Applied Physics Letters **93**(13) pp. 132103,1-3 (2008)

[21] G.A. Medvedkin ,Jpn. J. Appl. Phys., Part 2 39, p.L949 (2000)

[22] S.Sonoda, S.Shimizu, T.Sasaki, Y.Yamamoto and H.Hori, J.Cryst. Growth 237-239, p.1358 (2002)

[23] N.Theodoropoulou, A. F. Hebard, M. E. Overberg, C. R. Abernathy, S. J. Pearton, S. N. G. Chu, and R. G. Wilson, Phys. Rev. Lett. **89**, pp.107203,1-4 (2002)

[24] Y.Matsumoto *et al.*, Science (Washington, DC, U.S.) **291**, pp.854-856 (2001)

[25] F.Matsukura, H. Ohno and T.Dietl "III-V Ferromagnetic semiconductors" in Handbook of magnetic materials chapter edited by K.H.J. Buschow, Elsivier Science, (2003)

[26] T. Dietl, A.Haury and M. d'Aubigne, Phys.Rev. B **55**, pp.R3347-R3350 (1997)

[27] P. Wachter, CRC Crit. Rev. Solid State Sci. 3189 (1972)

[28] J.Szczytko, W.Mac, A.Twardowski, F.Matsukura and H.Ohno, Phys.Rev. B **59** pp.12935-12939 (1999)

[29] H. Ohno and F.Matsukura, Solid State Communications **117** pp.179-186 (2001)

[30] A. Van Esch, L. Van Bockstal, J De Boeck ,Phys.Rev. B **56**, pp.13103-13112 (1997)

[31] T. Dietl, H. Ohno, F. Mastukura, J. Cibert, and D. Ferrand, Science **287**, pp.1019-1022 (2000).

[32] C. Zener, Phys. Rev**. 83**, pp.299-301 (1951)

[33] G. Alvarez, M. Mayr, and E. Dagotto, Phys. Rev. Lett. **89**, pp.277202, 1-4 (2002).

[34] K. S. Burch D. B. Shrekenhamer, E. J. Singley, J. Stephens, B. L. Sheu, R. K. Kawakami, P. Schiffer, N. Samarth, D. D. Awschalom, and D. N. Basov , Phys. Rev. Lett. **97**, pp.087208, 1-4 (2006).

[35] M. A. Ruderman and C. Kittel, Phys. Rev. **96**, pp.99-102 (1954).

[36] W. K. Heisenberg, Z. Phys. **49**, p.619 (1928).

[37] H. Akai, Phys. Rev. Lett. **81**, pp.3002-3005 (1998).

[38] C. Zener, Phys. Rev. **82**, pp.403-405 (1951).

[39] M. S. Kim and C. H. Park, J. Korean Phys. Soc. **46**, pp.536-540 (2005).

[40] J. De Boeck *et al.*, J. Magn. Mater. **156**, pp.148-150 (1996).

[41] T.-B. Ng, D. B. Janes, D. McIntur, and J. M. Woodall, Appl. Phys. Lett. **69**(23),pp. 3551-3553 (1996).

[42] H. Ohno, Science **281**, pp.951-955 (1998).

[43] K. W. Edmonds *et al.*, Appl. Phys. Lett. **81**(16) pp. 3010-3012 (2002).

[44] O. Yastrubchak , Journal of Nano- and Electronic Physics **4**(1) pp. 01016, 1-6 (2012)

[45] T.Jungwirth, J. Sinova, A. H. MacDonald, B. L. Gallagher, V. Novák, K. W. Edmonds, A. W. Rushforth, R. P. Campion, C. T. Foxon, L. Eaves, E. Olejník, J. Mašek, S.-R. Eric Yang, J. Wunderlich, C. Gould, L. W. Molenkamp, T. Dietl, and H. Ohno.*,* Phys.Rev. B **76** pp.125206, 1-9(2007)

[46] A.L. Fetter and J.D. Walecka "Quantum Theory of Many-Particle Systems" New York; McGraw-Hill, 1971)

[47] P. Wachter, CRC Crit. Rev. Solid State Sci. **3** p.189 (1972)

[48] M.A. Dubson and D.F. Holcomb, Phys. Rev. B **32**, pp.1955-1960 (1985)

[49]S.M. Sze, "Physics of semiconductor devices "(Wiley, New York, 1981)

[50] W.A. Thompson, T.Penney, F.Holtzberg and S.Kirkpatrick, in Proceedings of the 11th International Conference on the Physics of Semiconductors (Polish Scientific, Warsaw, Poland, 1972) Vol.2, p.1255

[51] M.Reed *et al* , Applied Physics Letters **79** (21)pp.3473-3475 (2001)

[52] M.Tanaka and Y. Higo, Phys. Rev. Lett. **87**, pp.026602, 1-4 (2001)

[53] R.Mattana, J.-M. George, H. Jaffrès, F. Nguyen Van Dau, A. Fert, B. Lépine, A. Guivarc'h, and G. Jézéquel,Phys. Rev. Lett**. 90**, pp.166601, 1-4 (2003)

[54] C.Ruster, T.Borzenko, C.Gould, G.Schmidt , Phys.Rev.Lett. **91**, pp.216602, 1-4 (2003)

[55] C.Gould, C.Ruster, T.Jungwirth, E.Girgis, G.M.Schott, R.Giraud, K.Brunner, G.Schmidt and L.W. Molenkamp, Phys. Rev. Lett. **93**, pp.117203, 1-4 (2004)

[56] R.Giraud,M.Gryglas, L.Thevenard, A. Lemaitre and G.Faini,Appl. Phys. Lett. **87**(24),pp.242505,1-3 (2005)

[57] C.Ruster, C.Gould, T.Jungwirth, J.Sinova, G.M.Schott, R.Giraud, K.Brunner and L.W. Molenkamp, Phys. Rev. Lett. **94**, pp.027203, 1-4 (2005)

[58] A.D. Giddings, M.N. Khalid, T.Jungwirth, J.Wunderlich, S.Yasin, R.P Campion, K.W. Edmonds, J. Sinova, K.Ito, K.Y.Wang, D.Williams ,Phys. Rev. Lett. **94**, pp.127202, 1-4 (2005)

[59] L.Brey, C.Tejedor, J.Fernandez-Rossier ,Appl.Phys. Lett. **85** (11) pp.1996-1998 (2004)

[60] P.Sankowski, P.Kacman, J.A.Majewski, T.Dietl,Phys.Rev.B **75**, pp.045306,1-10 (2007)

[61] Y.Ohno, D.K.Young, B.Beschoten, F.Matsukura, H.Ohno and D.D.Awschalom, Nature (London) Vol. 402, issue 6763 pp.790-792 (1999)

[62]E.Jonston-Halperin, D.Lofgreen, R.K.Kawakami, D.K.Young, L. Coldren, A.C.Gossard and D.D. Awschalom, Phys.Rev. B **65** pp.041306, 1-4 (2002)

[63] P.Van Dorpe, Z.Liu, W. Van Roy, V.F. Motsnyi, M. Sawicki, G.Borghs and J De Boeck, Appl. Phys. Lett. **84** (18), pp.3495-3497 (2004)

[64] M.Kohda, T.Kita, Y.Ohno,F.Matsukura and H.Ohno, Appl. Phys. Lett. **89**(1), pp.012103,1-3 (2006)

[65] E.E. Mendez, L.Esaki, and W.I.Wang, Phys. Rev. B **33**, pp.2893-2896 (1986)

[66] R.K. Hayden, D.K. Maude, L.Eaves, E.C.Valadares, M. Henini, F.W.Sheard, O.H.Hughes, J.C.Portal and L.Cury, Phys.Rev.Lett. **66**, pp.1749-1752 (1991)

[67] H.Ohno, N.Akiba, F.Matsukura, A.Shen, K.Otani and Y.Ohno, Appl. Phys. Lett. **73** (3), pp.363-365 (1998)

[68] N.Akiba, F.Matsukura, Y.Ohno, A.Shen, K.Otani, T.Sakon, M.Matokawa and H. Ohno, Physica B 256-258, p.561 (1998)

[69] A.Haury, A.Wasiela, A.Arnoult, J.Cibert, S.Tatarenko, T.Dietl and Y.Merle d'Aubigne, Phys.Rev.Lett **79** pp.511-514 (1997)

[70] S.Nonoyama and J.Inoue, Physica E **10** (1), pp. 283-287 (2001)

[71] A.G.Petukhov, A.N.Chantis and D.O.Demchenko, Phys. Rev. Lett.**89**, pp.107205, 1-4 (2002)

[72] A.G.Petukhov, D.O.Demchenko and A.N.Chantis, J. Vac. Sci. Technol. B **18**, p.2109 (2000)

[73] A.G.Petukhov, D.O.Demchenko and A.N.Chantis, Phys.Rev. B **68**, pp.125332,1-5 (2003)

[74] R.Tsu and L.Esaki, Appl. Phys. Lett. **22** (11), pp.562-564 (1973)

[75]D.K.Ferri and S.M.Goodnick,"Transport in Nanostructures",Cambridge University Press,Cambridge, 1997

[76] D.E. Brehmer, K.Zhang, C.J.Schwartz, S.-P.Chau, S.J. Allen, J.P. Ibbetson, J.P. Zhang, C.J. Palmstrom and B. Wilkins, Appl. Phys. Lett**. 67** (9), pp.1268-1270 (1995)

[77] A.Slobodskyy, C.Gloud, T.Slobodskyy, C.R.Becker, G.Schmidt and L.W.Molenkamp, Phys.Rev Lett. **90**, pp.246601, 1-4 (2003)

[78] H.Mizute and T.Tanoue "The Physics and Applications of Resonant Tunnelling Diodes", Cambridge University press, Cambridge, 1995

[79]T.A.Foulton and G.S. Dolan, Phys. Rev. Lett. **59**, p.109 (1988)

[80] S.Doniah and E.H. Sondheimer, "Green's functions for Solid-State Physicists." W.A.Benjamin, Inc., 1974

[81] V.Igarashi et al., Phys.Rev. **B** 76, p.081303 (R) (2007)

[82] L.Besombes, Y.Leger, L.Maingault, D.Ferrand, H.Mariette and J.Gibert, Phys.Rev.Lett.**93**,p.207403 (2004)

[83] T.Gurund, S.Mackovski, L.M.Smith, H.E,Jackson, W.Heiss, J.Kossut and G.Karczewski, J.Appl.Phys.**96**, p.7407 (2004)

[84] S.Lee, M.Dobrovolska and J.K.Firdyna, Phys.Rev. B **72** p.075320 (2005)

[85] P.Wojnar, J.Suffczynski, K.Kowalik, A.Golnik, G.Karczewski and J.Kossut, Phys.Rev B **75**, p.155301 (2007)

[86] Y.Leger, L.Besombes, J.Fernandez-Rossier, L.Maingault and H.Mariette, Phys.Rev.Lett.**97**, 107401 (2006)

[87] R.M.Abolfath, P.Hawrylak and I.Zutic, Phys.Rev.Lett. **98**, p.207203 (2007)

[88] K.M.Hanif, R.W.Meulenberg and G.F. Strouse, J.Am. Chem. Soc. 124, p.11495 (2002)

[89] D.A.Schwartz, N.S.Norberg, Q.P. Nguyen, J.M.Parker and D.R.Gamelin, J.Am. Chem. Soc. **125**, p.13205 (2003)

[90] M.Holub, S.Chakrabarti, S.Fathpour, P.Bhattacharya, Y. Lei and S.Ghosh, Appl.Phys.Lett. **85**,p.973 (2004)

[91] J.Wunderlich, T.Jungwirth, B.Kaestner, A.C.Irvine, A.B.Shick, N.Stone, K.Y. Wang, U.Rana, A.D. Giddings, C.T. Foxon, R.P.Campion, D.A.Williams and B.LGallagher, Phys.Rev.Lett. **97**, p.077201 (2006)

[92]D. N.Zubarev "Nonequilibrium Statistical Thermodynamics" (Consultant Bureau, New York, 1974)

[93] C.Lacroix, J. Phys. F: Met. Phys. **11**, p.2389 (1981)

[94] Y.Meir, N.S.Wingreen and P.A.Lee, Phys.Rev.Lett **70**, p.2601 (1993)
 N.S.Wingreen and Y.Meir, Phys.Rev B **49**, 11040 (1994)
 Y.Meir, N.S.Wingreen and P.A.Lee Phys.Rev.Lett **66**, 3048 (1991)

[95] T.A. Costi, Phys.Rev. **B 64**, p.241310 (R) (2001)

[96] D.Goldhaber-Gordon, J.Gores, M.A.Kastner, H.Shtrickman, D.Mahalu and U.Meirav, Phys.Rev.Lett. **81**, 5225 (1998)

[97] S.M.Cronenwett, T.H. Oosterkamp and L.Kouvenhoven, Science **281**, 540 (1998)

[98] F.Simmel, R.H.Blick, J.P. Kotthaus, W.Wegscheider and M.Bichler, Phys.Rev.Lett. **83**,804 (1999)

[99] W.G. van der Wiel, S.De Franceschi, T.Fujisawa, J.M.Elzerman, S.Tarucha and L.P. Kouvenhoven, Science **289**, 2105 (2000)

BUSINESS +
ECONOMY

ART +
DESIGN +
ARCHITECTURE

SCIENCE +
TECHNOLOGY

CROSSOVER

DOCTORAL
DISSERTATIONS